

/ Faculteit Technische
Natuurkunde

Representing sub-grid scale plume
chemistry from shipping emissions in
Global Chemistry Transport Models

G.C.M. Vinken

R-1765-S

January 29, 2010

**Representing sub-grid scale plume
chemistry from shipping emissions in
Global Chemistry Transport Models**

G.C.M. Vinken

R-1765-S

January 29, 2010

Supervisors : Prof. Dr. D.J. Jacob (Harvard University, Cambridge, MA, USA)
Dr. K.F. Boersma (KNMI, de Bilt, The Netherlands)

Abstract

Due to instant dilution of ship emissions in grid cells and neglecting small-scale in-plume chemistry, current Chemistry Transport Models (CTMs) overpredict NO_x concentrations resulting from these emissions, and hence their ozone production. We adapted an existing Gaussian plume model with chemistry (PARANOX), originally built for aircraft emissions, to parameterize the sub-grid scale processes shortening the lifetime of NO_x in the plume. We updated the emissions, photolysis values for the boundary layer and plume dispersion in this model. Using this adapted PARANOX we were able to successfully simulate observations of a ship plume around noon near the Californian coast in May 2002. We showed that the NO_x concentrations after three hours already approach an enhanced background value, in accordance with observations. The NO_x lifetime found in the plume (around 2-3 hours) was lower than the background lifetime (of around 4-6 hours). In order to account for the sub-grid scale processes in global CTMs we parameterized the preprocessing step performed by PARANOX. We did this by running a stepwise linear regression for the fraction of NO_x remaining and the integrated Ozone Production Efficiency (OPE) on a large ensemble of environmental parameters for different location around the world in four different seasons. We split the parameterizations in four different equations, corresponding to four different photochemical regimes during the plume evolution, i.e. day, night, morning and evening. We found R^2 values above 0.8 for 6 out of 7 regressions, giving confidence in a good fit. The cross-variables ozone concentration ($[\text{O}_3]$) and ambient temperature (T) appear to be the most important in predicting the fraction of NO_x remaining during evening, night and morning. During the day, pressure explains most of the variance in the fraction of NO_x remaining. The positive relationship between the fraction of NO_x remaining and $[\text{O}_3]*T$ supposedly reflects a more efficient nighttime loss of NO_2 to NO_3 (and subsequently to HNO_3) in situations of high temperature and ozone concentrations. For the integrated OPE we found that in the morning the O_3 concentration is the most important variable, for day the temperature and for the evening the pressure. At night the integrated OPE equals zero, as there is no photochemical ozone production during the night. These results are important for better modeling ship emissions in CTMs and could prevent the over estimation of the fraction of NO_x remaining current models suffer from. Furthermore, as this parametrization is a simple formula it is easy portable between different models.

Contents

1	Introduction	1
2	Method	2
2.1	PARANOX model	2
2.1.1	Numerical approach of the Gaussian plume model	2
2.1.2	Chemistry	3
2.1.3	Plume dispersion	4
2.1.4	Emissions in PARANOX	5
2.2	Model output	5
2.2.1	OPE and instantaneous lifetime	5
2.2.2	Integrated OPE and fraction of NO _x remaining	6
2.3	Comparing with observations	6
2.4	Parametrization	6
3	Results	11
3.1	Validation with observations	11
3.1.1	Emissions Settings	11
3.1.2	Background settings	11
3.1.3	Results	12
3.1.4	OPE and instantaneous NO _x lifetime	15
3.2	Parametrization	16
3.3	NO _x remaining	16
3.3.1	Daytime	16
3.3.2	Nighttime	17
3.3.3	Morning	18
3.3.4	Evening	18
3.4	Integrated OPE	19
3.4.1	Daytime	19
3.4.2	Nighttime	19
3.4.3	Morning	19
3.4.4	Evening	19
4	Conclusion and Outlook	20
A	Chemistry Reactions	21
B	Regression Coefficients	24
B.1	Fraction of NO _x remaining	24
B.1.1	Daytime	24
B.1.2	Nighttime	24
B.1.3	Morning	24
B.1.4	Evening	24
B.2	Integrated OPE	28
B.2.1	Daytime	28
B.2.2	Morning	28
B.2.3	Evening	28
C	Statistical output from regressions	31
C.1	Fraction of NO _x remaining	31
C.1.1	Daytime	31
C.1.2	Nighttime	31
C.1.3	Morning	31
C.1.4	Evening	31

C.2	Integrated OPE	35
C.2.1	Daytime	35
C.2.2	Morning	37
C.2.3	Evening	37
	References	39

1 Introduction

Current global numbers of ocean going ships are about 90,000 vessels and are increasing with about 4% per year [Corbett et al., 2003]. Besides CO and CO₂, one of the other combustion products of these ships are nitrogen oxides (NO_x = NO + NO₂). Current estimates of the total NO_x emissions of shipping range between 3.23 - 6.51 Tg N per year, between 15-30% of total emissions [Corbett et al., 2007]. These emissions of ships have been shown to be of significant influence in the marine boundary layer [Kasibhatla et al., 2000] and on human health, by catalyzing ozone production and by PM2.5 pollution leading to cardiopulmonary disease and premature mortality [Corbett et al., 2007]. Surprisingly, the shipping industry is the only industrial sector not regulated under the Kyoto protocol or any other legislation in the open ocean. For ships in national waters, e.g. harbors, regulation exists constraining the emissions of SO₂ and NO_x and obligating ships to use different fuel than in the open ocean. To assess the impact of the shipping emissions, legislators rely on emissions inventories and model studies [Corbett et al., 1999, Eyring et al., 2005, Wang et al., 2008]. These model studies are performed using (global) Chemistry Transport Models (CTMs), which allow modeling the effect of ship emissions on the ambient concentrations in a grid cell. Most CTMs instantly dilute the ship emissions over the entire grid cell, with typical dimensions ranging from 2°x2.5° to 4°x5°. However, Davis et al. [2001] indicate, by comparing model output with observations, that the current global models overpredict the NO_x concentrations resulting from the emissions of ships, and hence their ozone production. Their study also showed that the NO_x lifetime in the plume could be greatly shortened by chemical processes promoted by ship plume emissions themselves. By instantly diluting the ship emissions in the CTM grid cells the model misses these sub-grid scale processes.

Several studies have used Lagrangian box models to study the effect of the sub-grid scale processes on the chemistry of the emissions (e.g. von Glasow et al. [2003] and Song et al. [2003]). Both studies show that the NO_x lifetime in the plume is about a factor 2.5 - 10 shorter than the lifetime of roughly 1 day used in the marine boundary layer by CTMs. Von Glasow et al [2003] calculated an overestimation of modeled ozone production of up to 50% due to the neglect of plume chemistry and dynamics. Chen et al. [2005] found, using observations from the 2002 NOAA ITCT airborne field campaign, indication of enhanced in-plume NO_x destruction, leading to much lower lifetimes than the background. Their study found underestimation of the in-plume NO_x loss rate by about 30%. A method to account for these in-plume effects is by pre-processing the actual emissions by a suitable parametrization based on a dispersion model that accounts for plume chemistry. For aviation, Meijer et al. [1997] used a Gaussian plume model with 10 rings and found a decreasing NO_x perturbation in the North Atlantic flight corridor at ~12 km of 15-55%. By using a Gaussian plume model with only 1 ring for ship NO_x emissions, Franke et al. [2008] found that their global model, using instant dilution, would overestimate ship induced ozone production by a factor of three. From their results they were not able to draw quantitative conclusions on the NO_x enhancement.

Till now no CTM takes into account these in-plume effects. The GEOS-Chem model [<http://acmg.seas.harvard.edu/geos/>] currently avoids the overestimation problem discussed above by replacing every emitted NO_x molecule by 10 molecules O₃ and 1 molecule HNO₃, based on an average ozone production of 10 found by Chen et al. [2005]. This approach is better than the other CTMs, but neglects the fact that there is no O₃ production at night, neglects effects of temperature and ambient concentrations on O₃-NO_x chemistry and results in no shipping NO_x in the marine boundary layer. In this study we will focus on parameterizing the sub-grid scale processes of the ship NO_x emissions by using an adapted version of the Gaussian plume model used by Meijer et al. [1997]. Using this parametrization in global Chemistry Transport Models, e.g. GEOS-Chem, would presumably lead to better modeling of ship emissions and could prevent the overestimation of NO_x remaining.

We describe the plume model, the adaptations we made and the method used for the parametrization in chapter 2. In chapter 3, we validate the model with observations from Chen et al. [2005], and present the results of the parametrization in the form of a regression formula. In chapter 4 we give a conclusion and outlook for further research.

2 Method

2.1 PARANOX model

In this study a Gaussian dispersion plume model, named PARANOX (PARAmetrization of Aircraft emitted NO_x), developed by Meijer et al. [1997], has been used. This model was originally designed for aircraft emissions in the high troposphere. The model simulates the chemical evolution of atmospheric trace gas concentrations resulting from aircraft emissions in time, as a cross-section of the plume, perpendicular to the wind direction. The model takes into account the chemistry within and outside of the plume, diffusion of emitted species inside the plume, expansion of the plume and entrainment of ambient air in the plume.

2.1.1 Numerical approach of the Gaussian plume model

The distribution of the concentrations in the ship plume is assumed to be Gaussian shaped. The concentration (kg/m³) of a species in the plume can be written as

$$C(x, y, z) = \frac{q}{2\pi u \sigma_y \sigma_z} \left[\exp\left(\frac{-y^2}{2\sigma_y^2}\right) + \exp\left(\frac{-z^2}{2\sigma_z^2}\right) \right] \quad (1)$$

With x the downwind distance from the emission source, y the crosswind distance, z the distance above the source, u the wind speed (m/s) along the plume centerline, q the emission (kg/s) and σ_y (m) and σ_z (m) the standard deviation of the statistical normal plume in lateral and vertical dimension, respectively. Note that σ_y and σ_z depend on x , as will be later described in section 2.1.3.

Since the chemistry of NO_x loss and ozone production is non-linear to the concentrations of NO_x, the Gaussian profile is discretized in 10 concentric elliptical rings in order to represent the distribution of concentrations within the plume. Exchange between neighboring rings and entrainment of ambient air through the outermost ring is allowed. To describe dispersion and turbulent mixing, a mass balance was formulated by Freiberg et al. [1976] and completed by Melo et al. [1978]. For a species j in ring i of the plume, this mass conservation equation equals:

$$\frac{dc_i^j(t)}{dt} = \lambda(\alpha_i c_{i-1}^j(t) + \beta_i c_i^j(t) + \gamma_i c_{i+1}^j(t)) + P_i^j(t, C) - L_i^j(t, C) c_i^j(t) \quad (2)$$

with $c_i^j(t)$ the concentrations of species j in ring i . The terms $P_i^j(t, C)$ and $L_i^j(t, C)$ are the chemical production and loss rates, with C the concentrations vector, containing the concentrations of all chemical species in the model. The coefficient λ describes the expansion of the plume and the depends on the area A of the cross-section of the plume by

$$\lambda = \frac{d \ln A}{d \ln t} \quad (3)$$

The coefficients α , β and γ are called Lusi coefficients and only depend on the number of rings chosen and are given by Melo et al. [1978] to be

$$\begin{aligned} \alpha_i &= \frac{1}{A_i} \frac{A_{i-1}}{A_i - A_{i-1}} \sum_{m=1}^{i-1} A_m \\ \gamma_i &= \frac{1}{A_i} \frac{A_{i+1}}{A_{i+1} - A_i} \sum_{m=1}^i A_m \\ \beta_i &= -(\alpha_i + \gamma_i) \end{aligned} \quad (4)$$

with A_i the surface of ring i , given by

$$A_i = 2\pi \sigma_y \sigma_z \ln \frac{N - i + 1}{N - i} \quad (5)$$

where N is the number of rings, and σ_y and σ_z the standard deviation of the statistical normal plume in lateral and vertical dimension, respectively. These plume variances are important parameters in describing the expansion of the plume and will be further discussed in section 2.1.3. The area of the outermost ring is set equal to twice that of the second outermost ring and the total surface of the cross-section is equal to

$$A(t) = \sum_{i=1}^N A_i = 2\pi\sigma_y\sigma_z \ln 4N \quad (6)$$

The number of rings N determines the fraction of the Gaussian plume that is described by the model. We used the model with 10 rings, resulting in $\sim 99.6\%$ of the exhaust incorporated in the model. Looking at equation (6) we see that the maximum radius of the plume in the horizontal and vertical direction equals

$$\begin{aligned} r_{max,y} &= \sqrt{2 \ln 40} \sigma_y = 2.71 \sigma_y \\ r_{max,z} &= \sqrt{2 \ln 40} \sigma_z = 2.71 \sigma_z \end{aligned} \quad (7)$$

Furthermore, the innermost ring cannot have fluxed inward, therefore $\alpha_1 = 0$. Likewise, the outermost ring has no outward flux, thus $\gamma_N = 0$.

The entrainment of ambient air into the plume is taken into account by adding an extra term to equation (2) for the outermost ring:

$$\frac{dc_i^N(t)}{dt} = \lambda(\alpha_N c_{N-1}^j(t) + \beta_N c_N^j(t)) + P_N^j(t, C) - L_N^j(t, C) c_N^j(t) + c_a^j \lambda \frac{\ln 4N}{\ln N} \quad (8)$$

with c_a^j the ambient concentration of species j .

2.1.2 Chemistry

The model includes a detailed simulation of tropospheric O_3 - NO_x -hydrocarbon chemistry for the troposphere, containing 44 species and 103 reactions. The reactions are given in Appendix A. The gas-phase reaction rates are taken from [DeMore et al., 1994]. The chemistry model is described in full detail by Meijer et al [1997]. Rainout of species is not taken into account. The photolysis values, which were originally only available for vertical levels between 7 and 13 km, have been taken from the GEOS-Chem model. The chemical timestep in the model is 100 seconds.

In the ship exhaust sulfate particles are formed, that could intensify heterogeneous processes in the plume with respect to the ambient air. The model includes heterogeneous formation of HNO_3 from N_2O_5 and H_2O on aerosols. The reaction rate constant K_{het} (s^{-1}) is given by

$$K_{het} = \frac{1}{4} \gamma \nu S \quad (9)$$

With γ the reaction probability, S (m^{-1}) the aerosol surface area density, and ν (ms^{-1}) the mean absolute molecular velocity of air particles. The reaction probability of N_2O_5 on sulphate aerosol is 0.1 in tropospheric conditions above 200K [DeMore et al., 1994]. More recent studies (e.g. Evans and Jacob [2005]) suggest lower values of 0.02 for this reaction probability. This parameter can be adapted to this value in future research.

The aerosol surface area density is determined by

$$S = 4\pi r_{SO_4}^2 [SO_4^{aerosol}] \quad (10)$$

with r_{SO_4} the radius of sulfate particles (0.015×10^{-4} cm) and $[SO_4^{aerosol}]$ the concentration of the SO_4 aerosols in the plume. The sulfate aerosols emissions are provided by the inventory given by Eyring et al. [2005].

The mean molecular velocity of air is determined by

$$\nu = \sqrt{(8. * R_{gas} * T) / (\pi * M_{air})} * 100 \quad (11)$$

with T the absolute temperature (K), R_{gas} the gas constant (8.3144 J/K/mol) and M_{air} the molar weight of air (0.002897 kg/mol).

To facilitate the discussion of the plume chemistry in the remaining report, the most critical $O_3/NO_y/HO_x$ reactions for both day and nighttime are given in Table 1. Note that in reaction [R1] the reactions with atomic oxygen ($O(^1D)$ and $O(^3P)$) are made implicit. This reaction is a net reaction of the loss of O_3 by photolysis to $O(^1D)$, followed by three possible reactions. The $O(^1D)$ can react with H_2O forming 2 OH molecules, the $O(^1D)$ can react with N_2 forming $O(^3P)$ and N_2 or the $O(^1D)$ can react with O_2 forming $O(^3P)$ and O_2 . From these last two possibilities, the $O(^3P)$ can react with O_2 producing O_3 . In reaction [R1] x_3 and x_4 are stoichiometric coefficients, quantifying the relationship of reactants and products in this net reaction. These stoichiometric coefficients are calculated in PARANOX and depend on temperature, N_2 concentrations, O_2 concentrations and H_2O concentrations.

Table 1: Most critical $O_3/NO_y/HO_x$ reactions for both day and nighttime.

R1	$O_3 + h\nu \xrightarrow{H_2O} x_3 OH + x_4 O_3 + O_2$
R2	$NO_2 + OH + m \rightarrow HNO_3 + m$
R3	$O_3 + NO \rightarrow NO_2 + O_2$
R4	$NO + HO_2 \rightarrow NO_2 + OH$
R5	$NO_2 + h\nu \rightarrow NO + O_3$
R6	$O_3 + NO_2 \rightarrow NO_3 + O_2$
R7	$NO_2 + NO_3 + m \rightarrow N_2O_5 + m$
R8	$CH_3O_2 + NO \rightarrow HCHO + HO_2 + NO_2$
R9	$NO_3 + h\nu \rightarrow NO_2 + O_3$
R10	$N_2O_5 + H_2O \xrightarrow{aerosol} 2HNO_3$

2.1.3 Plume dispersion

Originally, the lateral and vertical dispersion were described by vertical and horizontal diffusion coefficients, skewed diffusion and wind shear approximated in the high troposphere [Meijer et al, 1997]. In this study we decided to follow an approach for the lower troposphere originally described by Hanna et al. [1985] and adapted for dispersion calculations over water by Song et al [2003]. In this approach, the lateral and vertical dispersion are described by

$$\begin{aligned} \sigma_y &= 0.05x(1 + 0.0001x)^{-0.5} + \sigma_{y,0} & x \leq 10km \\ \sigma_y &= 0.05x(2)^{-0.5} + \sigma_{y,0} & x \geq 10km \\ \sigma_z &= 0.03x(1 + 0.0015x)^{-0.5} + \sigma_{z,0} \end{aligned} \quad (12)$$

with x the downwind distance from the source and $\sigma_{y,0}$ and $\sigma_{z,0}$ the initial lateral and vertical dispersion parameters. Both are typically given values of 5 meters in ship plume studies [Song et al., 2003]. In these equations we assume a ship-wind geometric configuration where the ship is moving perpendicular to the wind. Furthermore we assume ‘Neutral’ stability as meteorological stability class. This reflects water and air temperatures in the marine boundary layer being frequently close to equilibrium. In remote marine settings, a stability class can persist for sometimes even days. The marine boundary layer is often topped by an inversion at height h . It is generally assumed that plumes will not expand above this top. Therefore, we stop expansion in the vertical direction when the outer radius of the 10^{th} ring reaches this top, i.e. when $2.7\sigma_z = h$. After this top has been reached the expansion in the lateral direction still continues.

2.1.4 Emissions in PARANOX

The emissions in the model are treated as concentrations (molecules cm^{-3}) in the initial plume cross-section area. These emissions can be set in the model to the latest available inventories containing ship emissions.

To account for the plume being bounded below by the sea surface an image plume at $z = 0$ has been added, this has been done by doubling the initial concentrations in all rings, which are released at $t = 0$. Because the volume of this bounded plume is half the volume of the entire plume, we double the emissions. This is visualized in Figure 1.

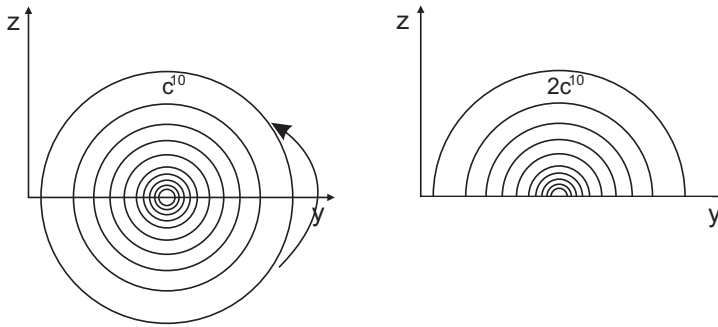


Figure 1: Figure showing the initial plume and the doubling of the initial concentrations.

2.2 Model output

2.2.1 OPE and instantaneous lifetime

As mentioned before, the main problem in the global models is the over prediction of NO_x in the plume due to too long lifetimes. In this study we define the NO_x lifetime within the plume in terms of how fast NO_x is lost at a given point in time, the so-called "instantaneous lifetime". The definition of the NO_x instantaneous lifetime is the NO_x concentration at any point in time divided by the NO_x loss rate. In this study we take the NO_x loss rate to be the production of HNO_3 . So the NO_x instantaneous lifetime is given by

$$\tau_{\text{NO}_x} = \frac{[\text{NO}] + [\text{NO}_2]}{P_{\text{HNO}_3}} \quad (13)$$

The main sink of NO_x during the day is reaction of NO_2 with OH via reaction [R2], i.e. the production of HNO_3 . At night it is mainly controlled by [R6] and [R7], which involve the formation of NO_3 and N_2O_5 , followed by HNO_3 formation by reaction of N_2O_5 on sulfate aerosols [R10].

An important concept in the production of O_3 by NO_x emissions is the Ozone Production Efficiency (OPE). The OPE is defined as the number of ozone molecules produced per molecule of NO_x consumed. In this study we again take the loss of NO_x to be equal to the production of HNO_3 , leading to

$$\text{OPE} = \frac{P_{\text{O}_3}}{P_{\text{HNO}_3}} \quad (14)$$

The OPE can be seen as the chain length in the chain mechanism producing O_3 from NO_x . A NO_x molecule emitted by the ship is involved in a number OPE of peroxy + NO reactions [R8], producing ozone [R5], before being converted to HNO_3 (mainly by [R2]). HNO_3 is the main sink for NO_x and removed by deposition. Our model does not take deposition into account, but the global CTM will solve removal by deposition eventually.

2.2.2 Integrated OPE and fraction of NO_x remaining

In order to use the ship plume model in global CTMs two new output parameters have been added to the ship plume model; the fraction of NO_x remaining and the integrated OPE. The fraction of NO_x remaining is determined by dividing the mass of NO+NO₂ in the plume at time t by the mass of NO+NO₂ in the plume at time $t = 0$. To calculate this fraction of NO_x remaining in a clean way the entrainment of ambient NO_x, PAN and HNO₃ has been disabled in the parametrization. The fraction of NO_x remaining can be used to reduce the initial amount of NO_x upon release at time t in the global CTM with the coarse spatial resolution.

The OPE described in the previous section can be regarded as an "instantaneous OPE". When using the ship plume model as a pre-processor for the ship emissions we need to assess the OPE during the entire plume expansion. For this reason we introduce the "integrated OPE". This integrated OPE (Ω) is determined by the ratio of the total ozone produced and the total NO_x lost (again as HNO₃ produced), i.e.

$$\Omega = \frac{\int_{t'=0}^t P_{O_3} dt'}{\int_{t'=0}^t P_{HNO_3} dt'} \quad (15)$$

in which t is the end time of the model (order of several hours).

2.3 Comparing with observations

In order to validate the simulations by the plume model we compare our results with observations from the ITCT 2k2 ship plume experiment, described by Chen et al. [2005]. To compare the results we have spun-up the ship plume model for 48 hours and then ran the plume expansion/chemistry for 3 hours, after initial release at 12.00 pm local time, consistent with the 3-hour period during which the measurements of an aging ship plume were taken. Output plots have been created for the O₃, NO_x and OH concentrations that have been measured and modeled, the OPE and the instantaneous lifetime. These will be discussed in Section 3.

2.4 Parametrization

One way to account for the sub-grid processes in global models is by parametrization of the fraction of NO_x remaining and the integrated OPE. The parametrization can be better understood by looking at Figure 2 and 3. Originally, the ship emissions are instantly diluted in the grid cell of the Global Model. In our approach, the ship plume model (PARANOX) preprocesses the emissions before we insert them in the Global Model grid cell. We shall create a parametrization for this preprocessing step.

This can be done by calculating the fraction of NO_x remaining and the integrated OPE as a function of environmental parameters. We used the GEOS-Chem chemistry-transport model to generate an ensemble of possible environmental parameters, which will be used as boundary conditions for the ship plume model. For creating this ensemble we used version v8-02-01 of the GEOS-Chem model [<http://acmg.seas.harvard.edu/geos/>]. We ran the model to output hourly concentrations (O₃, CO, H₂O₂, HNO₃, PAN, CH₂O, OH and H₂O), meteorological parameters (mixing depth, wind speed, temperature, density and pressure) and photolysis values for 1 January, 1 April, 1 July and 1 October. The ship plume model was then run for a number of emission strengths and the environmental conditions given by this ensemble. We subsequently stored the fraction of NO_x remaining, the integrated OPE, the month, time of release, solar elevation angle, ship emissions and the environmental parameters.

PARANOX was run for 5 hours for all the grid cells. This run time is an important parameter in the PARANOX model. Choosing it too short might lead to a too high fraction of NO_x remaining and thus too much ozone production when diluted back into the global model. Choosing it too long will effectively dilute NO_x emissions to values barely above background levels. A parameter that is also influenced by the run time is the size of the plume. Two figures of the time development

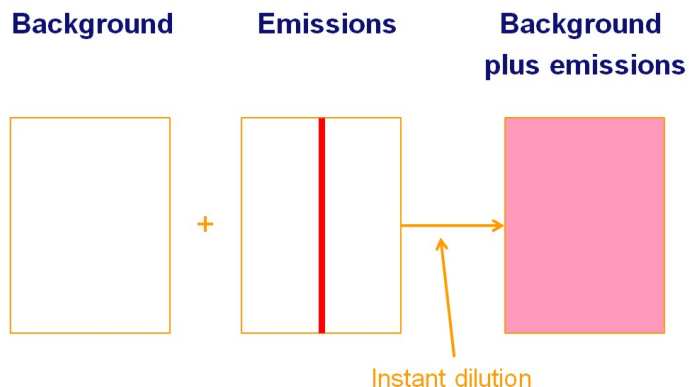


Figure 2: Figure illustrating the instant dilution of the emissions in a Global Model. The yellow rectangle represents one model grid cell. The white in the Global Model grid cell (left) reflects background model concentrations. The red line in the ‘emissions scenario’ (middle) indicates localized emissions along shipping lanes. The right cell illustrates the resulting dilution of local emissions with the clean background as enhanced, pink concentrations.

of the horizontal and vertical plume size for different wind speeds are given in figures 4(a) and 4(b), in this case assuming a boundary layer height of 500 m. As can be seen in the figures, after 2 to 3 hours the vertical plume size has reached the top of the boundary layer. When this point is reached we can assume the plume to be well-mixed vertically. We chose 5 hours in our runs as this will also allow the plumes to be well dispersed for higher mixing depths and the fast chemistry will have occurred within this timeframe. As we will see later in Figure 7, in 3 hours we already approach an enhanced background value. The horizontal plume size will be in the order of 10 kilometers, reducing the effect of dilution in the GEOS-Chem grid cell of size order 200 by 250 km.

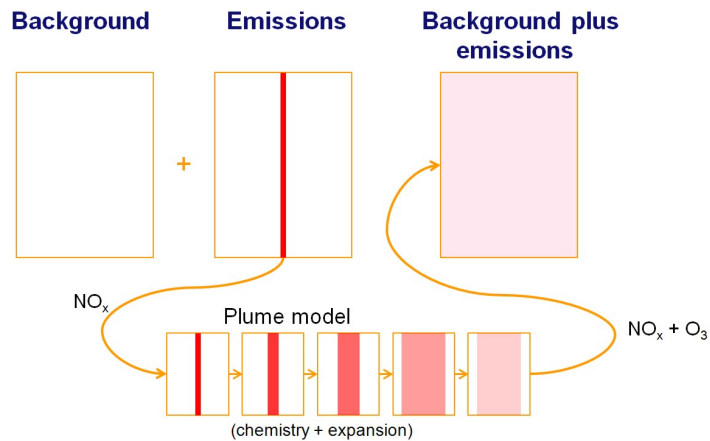
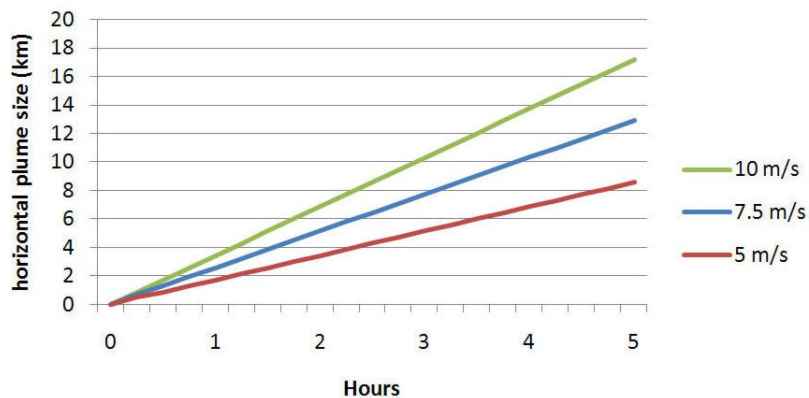
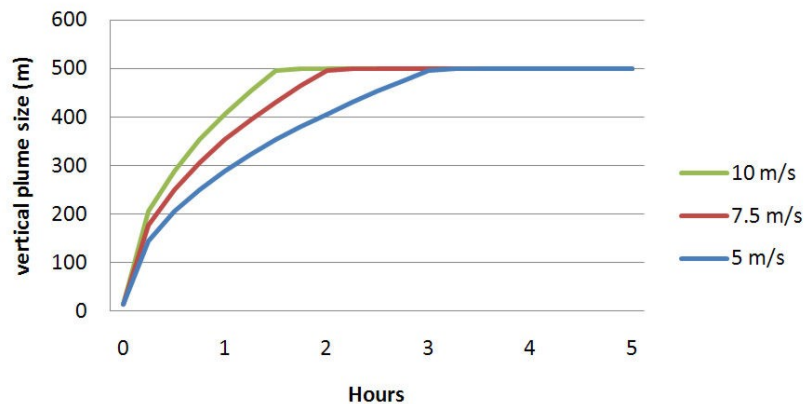


Figure 3: Figure showing the preprocessing of the emissions before inserting them in the Global Model (GM) grid cell. Now the plume model has preprocessed the emissions such that actual in-plume chemistry has been taken into account and results in lower (light pink) enhanced concentrations.



(a) Horizontal plume size.



(b) Vertical plume size.

Figure 4: Graph showing the dependence of the horizontal and vertical plume size on time for different wind speeds.

The ship NO_x emissions have been taken from the AMVER-ICOADS database described by Wang et al. [2008]. This database only gives NO_x emissions. A regridded map at $2^\circ \times 2.5^\circ$ of this inventory for January is given in Figure 5. Other emitted species (e.g. CO and CH_4) are taken from Eyring et al. [2005] and Hobbs et al. [2000]. Because we only know the spatial distribution of the NO_x emissions, we scale the other emitted species by the ratio of the NO_x emissions at a certain grid cell and the NO_x emissions given by Eyring et al. [2005].

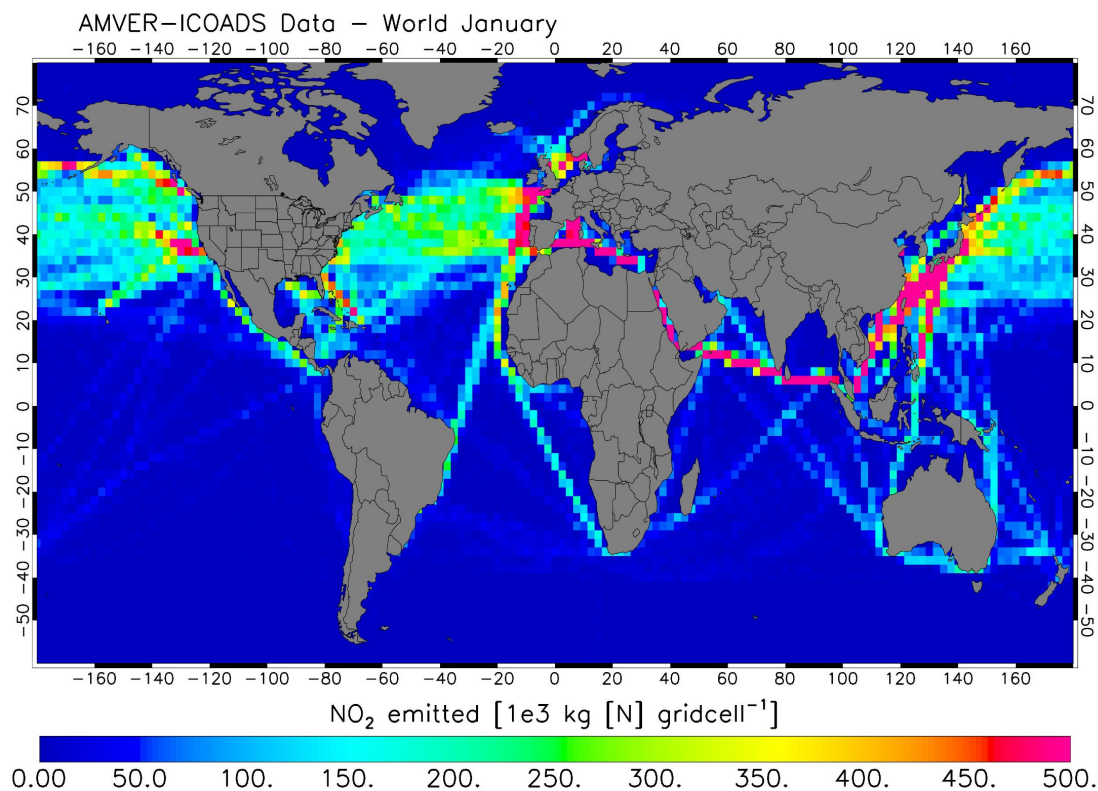


Figure 5: Regridded map at $2^\circ \times 2.5^\circ$ of the AMVER-ICOADS database for January indicating the total NO_2 emitted in $1\text{E}3$ kg N per grid cell.

To create the actual parametrization for the fraction of NO_x remaining and the integrated OPE we used the software program R [Hornik, 2009]. We use a stepwise linear regression, including first order interaction terms.

In the parametrization we only use values at the end of the 5 hour PARANOX run. By choosing this method, we do not have to save variables during the run of the global model later on. The only problem that arises using this method occurs at the terminator. For instance, a photolysis value of 0 at the end of the run does not tell us if the photolysis value has been nonzero at some point during the last 5 hours. The same problem occurs in the morning when the sun rises. To solve this problem we added the variables ‘solar elevation angle at endpoint’ and ‘solar elevation angle 5 hours ago’. These extra variables give us more information on the history of the j-values and enable us to separate the parametrization into day, night, morning and evening equations.

For day we require both the solar elevation angle at $t = 0$ and $t = 5$ hours to be positive. Both solar elevation angles being negative indicate that the grid cell was in darkness all 5 hours (night). If the solar elevation angle at $t = 0$ was negative and at $t = 5$ positive, then we classify this grid cell as being in the morning. For evening, the solar elevation angle at $t = 0$ has to be positive and the solar elevation angle at $t = 5$ has to be negative. We intend to capture the hours in darkness (or light) problem by regressing on the sign and magnitude of the solar elevation angles at $t = 0$ and at $t = 5$. For example, a run which has been 1 hour in light and 4 hours in darkness has a lower value of the solar elevation angle at $t = 0$ than a run which has been 4 hours in light and 1 hour in darkness. For the latter run, the value of the solar elevation angle at $t = 5$ would be larger (less negative) than the first example.

As possible dependent variables in the stepwise regression we used the variables given in Table 2.

Table 2: Dependent variables we used in the stepwise regression.

Variable	Indicated as
Wind speed	α
Temperature	β
J(NO ₂)	γ
Concentration(O ₃)	δ
Solar Elevation Angle at start point	ϵ
Solar Elevation Angle at endpoint	ζ
Emissions	η
J(O ₁ ^D) / J(NO ₂)	θ
Concentration(CO)	ι
Pressure	κ
Mixing depth	λ

3 Results

3.1 Validation with observations

We compare our ship plume model with observations given by Chen et al. [2005]. In this study measurements from a ship emission plume experiment 100 km off the Californian coast during the 2002 NOAA ITCT airborne field campaign were taken and compared with photochemical model calculations. The measurements were taken around noon on 8 May 2002. Measurements of chemical species were made from the NOAA WP-3D aircraft at ~ 100 m above sea level in eight consecutive transects of a ship plume, with the letters A-H in figure 6 corresponding to plume ages of 30 minutes (A) up to 3 hours (H). The measured species include NO_x , HNO_3 , PAN, SO_2 , H_2SO_4 , O_3 , CO and CO_2 . The flight path showing the transects of the ship plume is given in figure 6.

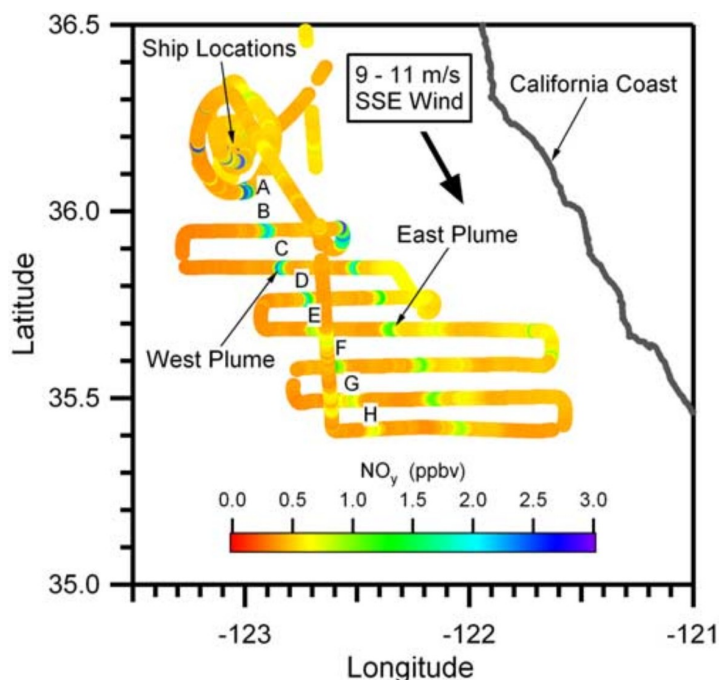


Figure 6: Flight path showing the transects of the ship plume, with the letters A-H corresponding to plume ages of 30 minutes (A) up to 3 hours (H).

3.1.1 Emissions Settings

The emissions used in the PARANOX simulation for comparison with the observations are given in Table 3. These emissions are derived from the inventory by Eyring et al. [2005] for cargo ships and from Hobbs et al. [2000].

The NO_x emissions are distributed as 94% NO and 6% NO_2 , as suggested by EPA [2000]. The ship speed is set to 5 m/s (9.7 knots), as used in Chen et al. [2005].

3.1.2 Background settings

The background settings for the comparison with the observations are taken from [Chen et al., 2005] and given in Table 4. These concentrations were measured during the ITCT 2k2 ship plume experiment, outside of the shipping plume around noon on 8 May 2002 about 100km off the Californian coast.

Species	Emissions (g/s)
NO _x	33
CO	0.98
SO ₂	20
SO ₄	0.58
CH ₄	0.16
Ethene	0.26
Propene	0.28
Xylene	0.05
H ₂ O	950

Table 3: Emissions from ships derived from Eyring et al. [2005] and Hobbs et al. [2000]

Species	Ambient Concentration (ppbv)
O ₃	42
NO	0.020
NO ₂	0.120
HNO ₃	0.005
CO	140
SO ₂	0.4
PAN	0.16
CH ₃ CHO	0.1
CH ₃ OH	0.25
H ₂ O ₂	0.28
CH ₃ OOH*	0.66
CH ₄ *	1743
HCHO*	0.32

Table 4: Ambient concentrations used in comparison with Chen et al. [2005]. *Values derived from original TM3 input in PARANOX model for lowest level.

PARANOX has been tuned to the NO_x background values shown in Table 4 by emitting a small NO_x puff every 100 seconds in the background.

During the measurements the wind speed was between 9 and 11 m/s, in this comparison we set the wind speed to 10 m/s. The height of the marine boundary layer determined from aircraft measurements was 350 m.

3.1.3 Results

The plot of the concentrations of NO_x, O₃ and OH as function of the time are given in Figure 7, 8 and 9. The concentrations represent the weighted average over the rings and can be thought of as representative for typical boundary layer concentrations.

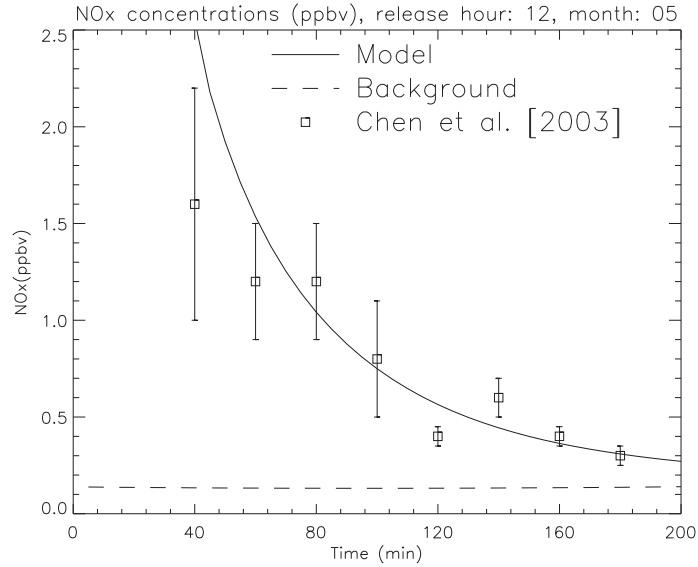


Figure 7: NO_x concentrations in the plume as function of time. The solid line indicates the PARANOX simulation with emissions as specified in Table 3 and ambient concentrations given by Table 4. The dashed line represents the background concentrations and the squares are the observation given by Chen et al. [2005] with the bars indicating the errors in these observations.

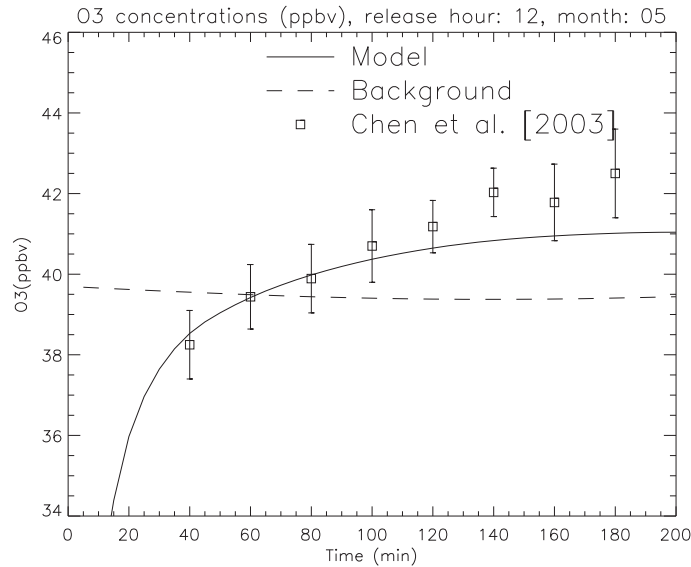


Figure 8: O₃ concentrations in the plume as function of time. The solid line indicates the PARANOX simulation with emissions as specified in Table 3 and ambient concentrations given by Table 4. The dashed line represents the background concentrations and the squares are difference between the observations and the observed background given by Chen et al. [2005] added to our background, with the bars indicating the errors in these observations.

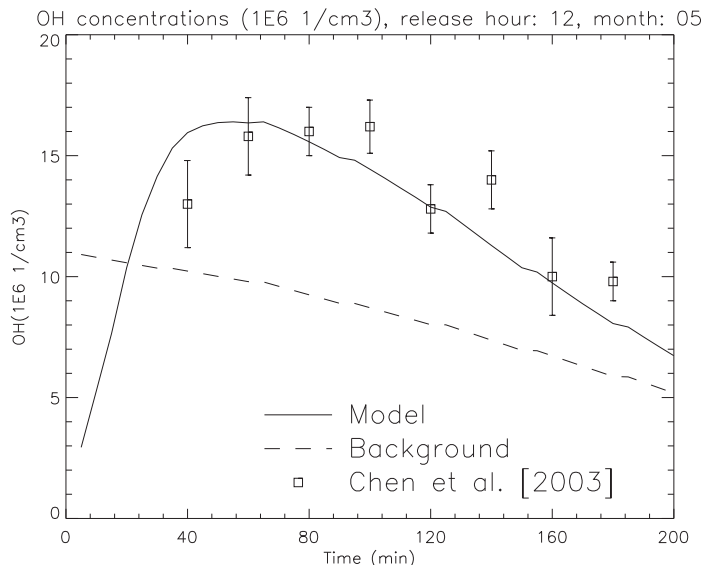


Figure 9: OH concentrations in the plume as function of time. The solid line indicates the PARANOX simulation with emissions as specified in Table 3 and ambient concentrations given by Table 4. The dashed line represents the background concentrations and the squares are the observation given by Chen et al. [2005] with the bars indicating the errors in these observations.

To structure the discussion of the plot results we separate the plume dispersion in three regimes, as proposed by [Song et al., 2003]. These regimes are: (1) early plume dispersion ($[\text{NO}_x]$ above 1 ppm); (2) midrange dispersion ($[\text{NO}_x] \sim$ several ppb) and (3) long-range dispersion ($[\text{NO}_x]$ below 1 ppb). From the O_3 plot we see that there is also another classification to express the evolution of the plume by the O_3 levels: (1) O_3 titration, (2) O_3 recovery, and (3) net O_3 production.

Stage (1) is rather short in this plume because the NO_x levels drop below 1 ppm within a few minutes after the release. The strong decline in the O_3 concentrations is caused by the O_3 being titrated by the abundantly available NO via reaction [R3]. Almost all O_3 is gone at this point, but stored as NO_2 and will later be recycled.

When the NO_x concentrations approach the values corresponding to stage (2), after 30 to 60 minutes, different reactions become dominant. Using the available NO , HO_2 is converted to OH and NO_2 via reaction [R4] (this can be seen by the rise in OH concentrations). The NO_2 is then photolyzed [R5], thus leading to net photochemical O_3 production. This stage is important in the problem of instantly diluting the emissions, as the OH concentrations are maximal in this stage and almost 8 times higher than background levels. This high OH concentration causes a shorter NO_x lifetime and a relatively low fraction of NO_x remaining. By instantly diluting the emissions the global model, this stage would be missing and leading to higher NO_x lifetimes.

With NO_x concentrations dropping below 1 ppb the final stage (3) sets in. Reactions of NO with HO_2 [R4] and organic peroxides (e.g. CH_3O_2 [R8]), lead to increasing levels of photochemically produced O_3 .

Our ship plume model seems to be able to simulate the observed values quite well. It must be noted that Chen et al. [2005] uses a constant background OH value of $6 \times 10^6 \text{ mol/cm}^3$, while we do not fix this value but simulate the diurnal variation in the concentrations. Furthermore the observations in the O_3 plot are the observed difference with the background by Chen et al. [2005] imposed on our background values. This is done because Chen et al. [2005] used fixed background O_3 values, while we simulate a diurnal variation in the O_3 concentrations. The observed OH concentrations are derived by Chen et al. [2005] from H_2SO_4 measurements, assuming that the source of H_2SO_4 is the OH initiated oxidation of SO_2 and it has short lifetime (~ 5 minutes) due

to aerosol scavenging.

3.1.4 OPE and instantaneous NO_x lifetime

The Ozone Production Efficiency and the instantaneous NO_x lifetime are given in figure 10 and 11.

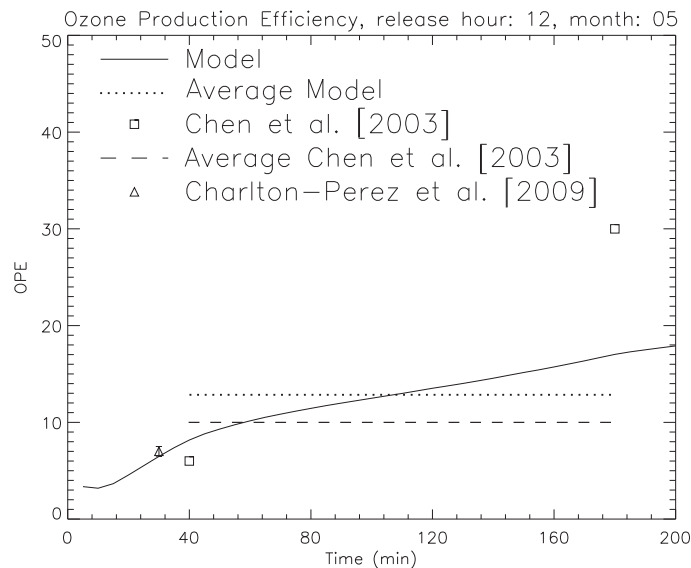


Figure 10: OPE in the plume as function of time. The solid line indicates the PARANOX simulation with emissions as specified in Table 3 and ambient concentrations given by Table 4, with the dotted line the average between 40 and 180 minutes. The squares are the observation given by Chen et al. [2005] with the dashed line representing the average between 40 and 180 minutes. The triangle is the modeled value found by Charlton-Perez et al. [2009] after 30 minutes after releasing a plume at noon.

Chen et al. [2005] only mentions two observations of the OPE, at 40 and 180 minutes. Furthermore they mention an average value of 10 in this timeframe. We find this value somewhat surprising when considering the values of 6 and 30 at 40 and 180 minutes, respectively. However, Chen et al. [2005] does not mention how this average value of 10 is calculated. As can be seen our plume model does not reproduce the exact values found by Chen et al. [2005] but the average value of 10 corresponds with our value of about 13. Furthermore, if we compare our modeled OPE with the values found by Charlton-Perez et al. [2009] for comparable plume size, our value at 30 minutes after release seems to agree with their value of about 7 for an 30 minutes old plume.

The NO_x lifetime in the plume is lower than in the background lifetime, which is already lower than in the pristine marine boundary layer (typically around 24 hours) due to the moderately polluted background near the Californian coast. In Chen et al. [2005] a constant background value of 6 hours is found, again related to the absence of diurnal variations in the simulations. This constant value of ambient OH could also be the reason for the higher lifetime at 180 minutes found in our plume model, as OH is the main sink of NO_2 .

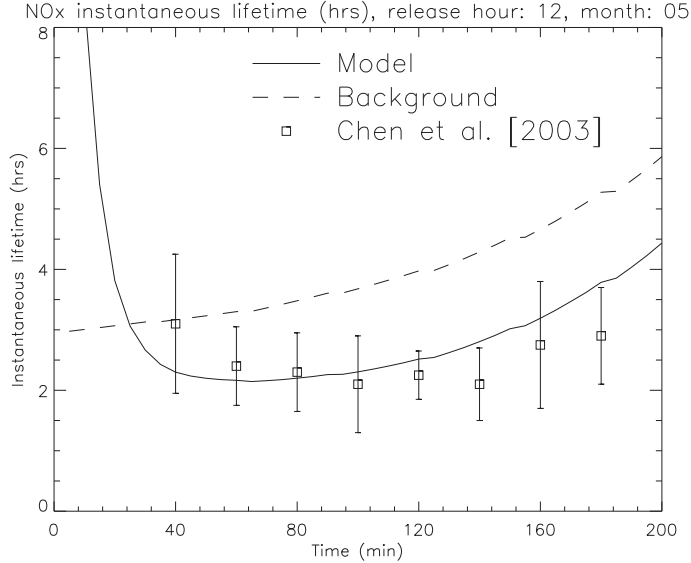


Figure 11: NO_x instantaneous lifetime in the plume as function of time. The solid line indicates the PARANOX simulation with emissions as specified in Table 3 and ambient concentrations given by Table 4. The dashed line represents the background concentrations and the squares are the observation given by Chen et al. [2005] with the bars indicating the errors in these observations.

3.2 Parametrization

We performed a stepwise linear regression on the data set provided by PARANOX with GEOS-Chem input. We did this to correlate the fraction of NO_x remaining and the integrated OPE to the parameters listed in 2. The general equation we found for this regression is

$$\Phi = \left(\begin{bmatrix} A_0 & A_1 & A_2 & \cdots & A_{11} \\ 0 & 0 & A_{1,2}\alpha & \cdots & A_{1,11}\alpha \\ \vdots & & \ddots & & \\ 0 & \cdots & \cdots & 0 & A_{10,11}\kappa \end{bmatrix} \begin{pmatrix} 1 \\ \alpha \\ \vdots \\ \kappa \\ \lambda \end{pmatrix} \right) \cdot \begin{pmatrix} 1 \\ 1 \\ \vdots \\ 1 \\ 1 \end{pmatrix}.$$

This regression formula is valid for all regressions we performed, with regression coefficients given in Appendix B.

3.3 NO_x remaining

3.3.1 Daytime

The regression coefficients A_i we found using a stepwise linear regression for the fraction of NO_x remaining (Φ) during daytime are given in Table 5 in Appendix B. From these coefficients, we see that the most important variables driving the fraction of NO_x remaining are 1) pressure, 2) the crossterm of pressure and temperature and 3) temperature. Furthermore we see that the emissions, mixing depth and solar elevation angle at $t = 0$ have no direct effect. However, there are indirect effects of these factors, for example the crossterm of wind speed and emissions. In Figure 12 the fraction of NO_x remaining is given as function of temperature*pressure, the second most important variable in the regression. In the plot it can be seen that a higher temperature*pressure leads to a lower fraction of NO_x remaining, as suggested by the regression. Because of all the other interactions of the variables it is hard to get a clear plot of the dependencies, we only used data with emissions > 20 g/s, 0.4 km $<$ mixing depth < 0.6 km and wind speed > 5 m/s. The positive temperature*pressure relationship that we find possibly reflects the

fact that high temperature and high pressure reflect good weather, high OH concentrations and hence fast chemistry, resulting in a low fraction of NO_x remaining. Low temperature and low pressure reflect a slower chemical regime, resulting in a high fraction of NO_x remaining.

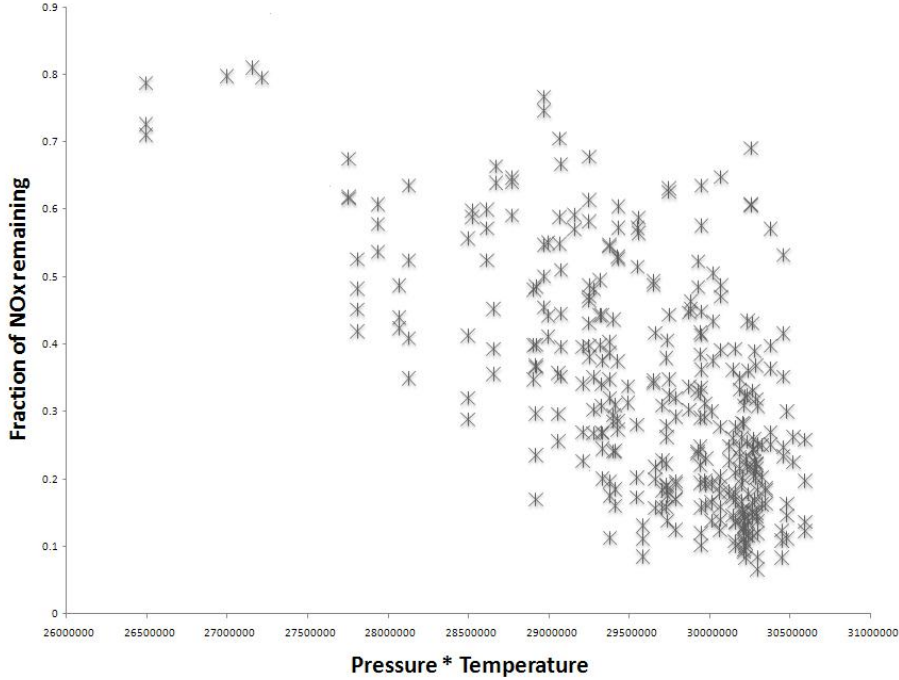


Figure 12: Fraction of NO_x remaining as function of temperature*pressure. For this plot only data points satisfying emissions > 20 g/s, 0.4 km $<$ mixing depth < 0.6 km and wind speed > 5 m/s have been used, resulting in 358 data points.

The R^2 of this regression was 0.83 with 7502 data points. The full statistical output can be found in Appendix C. Many cross terms are involved in the parametrization. We also tried the parametrization without the cross terms and this resulted in a R^2 of only 0.74, so it is better to include the cross terms in the parametrization.

3.3.2 Nighttime

The regression coefficients B_i we found using a stepwise linear regression for the fraction of NO_x remaining (Φ) during nighttime are given in Table 6 in Appendix B. From these coefficients, we see that the most important variables driving the fraction of NO_x remaining are 1) the crossterm of O_3 concentrations ($[\text{O}_3]$) and temperature (T), 2) the O_3 concentrations and 3) the crossterm of wind and temperature. Furthermore we see that the $J(\text{NO}_2)$, $J(\text{O}_1^D)/J(\text{NO}_2)$ and CO concentration have no direct effect. However, there are indirect effects of CO concentrations for example the crossterm of wind speed and CO concentrations. As expected, the variables ($J(\text{NO}_2)$ and $J(\text{O}_1^D)/J(\text{NO}_2)$) play no role in this regression, as they are zero in darkness. In Figure 13 the fraction of NO_x remaining is given as function of O_3 concentrations * temperature ($[\text{O}_3]*T$), the most important variable in the regression. In the plot it can be seen that a higher $[\text{O}_3]*T$ leads to a lower fraction of NO_x remaining, as is found by the regression. To reduce scatter, we only used data that satisfied 4 m/s $<$ wind speed < 6 m/s. We hypothesize that the positive $[\text{O}_3]*T$ relationship reflects the fact that that high O_3 concentrations influence the loss of NO_2 to NO_3 via [R6] and that high temperatures further increase the loss of NO_2 to NO_3 (and subsequently to N_2O_5 and HNO_3). Low temperatures and low O_3 concentrations would then indicate a chemically less active regime, where less NO_x is lost.

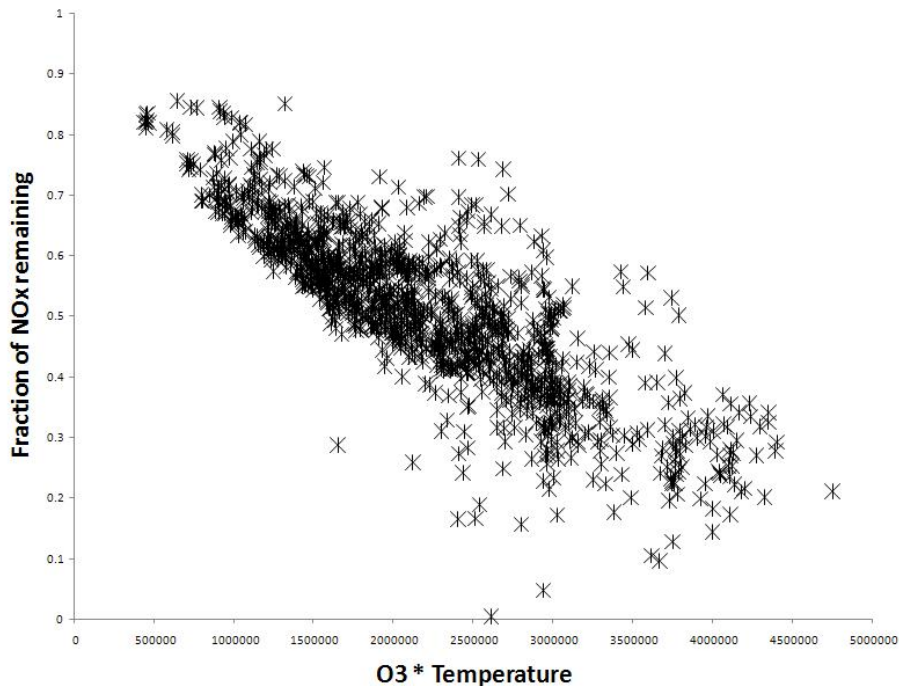


Figure 13: Fraction of NO_x remaining as function of O_3 concentrations * temperature. For this plot only data points satisfying $4 \text{ m/s} < \text{wind speed} < 6 \text{ m/s}$ have been used, resulting in 1333 data points.

The R^2 of this regression was 0.88 with 4264 data points. The full statistical output can again be found in Appendix C. Again we see a lot of terms, however fewer than in the daytime regression. We tried reducing the variables by excluding the cross terms, resulting in a R^2 of 0.82, which is still a good value.

3.3.3 Morning

The coefficients C_i we found using a stepwise linear regression for the fraction of NO_x remaining (Φ) during morning conditions are given in Table 7 in Appendix B. From these coefficients, we see that the most important variables driving the fraction of NO_x remaining are 1) the crossterm of O_3 concentrations ($[\text{O}_3]$) and temperature (T), 2) the O_3 concentrations and 3) the crossterm of wind and temperature, which is the same as for the night. Furthermore we see that the temperature, solar elevation angle at $t = 0$, $J(\text{O}_1^D)/J(\text{NO}_2)$, CO concentration and pressure have no direct effect. However, there are indirect effects of all the afore mentioned variables, except CO concentrations and pressure.

The R^2 of this regression was 0.84 with 3628 data points. The full statistical output can again be found in Appendix C.

3.3.4 Evening

The coefficients D_i we found using a stepwise linear regression for the fraction of NO_x remaining (Φ) during evening conditions are given in Table 8 in Appendix B. From these coefficients, we see that the most important variables are 1) the crossterm of O_3 concentrations ($[\text{O}_3]$) and temperature (T), 2) the crossterm of temperature and solar elevation angle at $t = 0$ and 3) the solar elevation angle at $t = 5$, CO concentration and pressure have no direct effect. However, there are indirect effects of all the afore mentioned variables, except pressure.

The R^2 of this regression was 0.82 with 4262 data points. The full statistical output can again be found in Appendix C.

3.4 Integrated OPE

3.4.1 Daytime

The coefficients E_i we found using a stepwise linear regression for the integrated OPE (Ω) during daytime are given in Table 9 in Appendix B. From these coefficients, we see that the most important variables are 1) the temperature, 2) the crossterm of O_3 concentrations and pressure and 3) the $J(NO_2)$ values. Furthermore we see that $J(O_1^D)/J(NO_2)$ and the mixing depth have no direct effect. However, there are indirect effects of both variables, for example the cross term of temperature and mixing depth.

The R^2 of this regression was 0.82 with 7500 data points. The full statistical output can again be found in Appendix C. We again tried the parametrization without the cross terms and this resulted in a R^2 of only 0.68, so again we conclude that it is better to include the cross terms.

3.4.2 Nighttime

The integrated OPE for night time is zero, as no O_3 can be photo chemically produced.

3.4.3 Morning

The coefficients F_i we found using a stepwise linear regression for the integrated OPE (Ω) during morning conditions are given in Table 10 in Appendix B. From these coefficients, we see that the most important variables are 1) the O_3 concentrations, 2) the crossterm of O_3 concentrations and pressure and 3) the crossterm of solar elevation angle at $t = 5$ and pressure. Furthermore we see that the wind speed, temperature, solar elevation angle at $t = 0$ and pressure have no direct effect. However, there are indirect effects of all the afore mentioned variables, except temperature. The R^2 of this regression was 0.71 with 3620 data points. The full statistical output can again be found in Appendix C.

3.4.4 Evening

The coefficients G_i we found using a stepwise linear regression for the integrated OPE (Ω) during evening conditions are given in Table 11 in Appendix B. From these coefficients, we see that the most important variables are 1) the pressure, 2) the crossterm of O_3 concentrations and pressure and 3) the crossterm of mixing depth and pressure. Furthermore we see that the wind speed, temperature, $J(NO_2)$, O_3 concentrations, solar elevation angle at $t = 5$ and emissions have no direct effect. However, there are indirect effects of all the afore mentioned variables.

The R^2 of this regression was 0.85 with 4255 data points. The full statistical output can again be found in Appendix C. We see that the R^2 of the evening regression is higher than the morning regression. We attribute this to the photochemical regime that is generally more favorable for ozone production in the late afternoon (higher temperature and well developed boundary layer) than in early morning (lower temperature and minimal boundary layer).

4 Conclusion and Outlook

Current global models overpredict the NO_x concentrations resulting from the emissions of ships, and hence their ozone production. Due to sub-grid scale processes, the NO_x lifetime in a shipping plume is shorter than the lifetime simulated by current CTMs that instantly dilute the ship emissions in the CTM grid cells. In this study we focussed on parameterizing these sub-grid scale processes of the ship NO_x emissions.

We adapted an existing Gaussian plume model with chemistry (PARANOX) originally built for aircraft emissions. We updated the values for emissions, photolysis and plume dispersion to values relevant for the marine boundary layer. Furthermore we added the ozone production efficiency (OPE) and instantaneous NO_x lifetime to the output of the model.

Using this adapted PARANOX we were able to successfully simulate observations of atmospheric composition in a ship plume near the Californian Coast in May 2002. We showed agreement between observed and simulated NO_x concentrations in the three hours after emissions. The NO_x lifetime found in the plume (around 2-3 hours) is lower than the background lifetime (of around 4-6 hours).

In order to account for the sub-grid scale processes in global CTMs we parameterized the preprocessing step performed by PARANOX. Using PARANOX we calculated the fraction of NO_x remaining and the integrated OPE (after 5 hours) for a large ensemble of environmental parameters for different locations around the world in four different seasons. The run time was chosen long enough that fast chemistry in the plume is done and short enough that NO_x emissions are still above background levels. Using a stepwise multiple linear regression on this data set we created a parametrization for the fraction of NO_x remaining and the integrated OPE based on ten different dependent variables: $J(\text{NO}_2)$, $J(\text{O}_1^D) / J(\text{NO}_2)$, mixing depth, wind speed, temperature, pressure, O_3 concentration, CO concentration, solar elevation angle at release time, solar elevation angle at endpoint and the NO_x emissions. We split the parametrization in four different equations, corresponding to four different light regimes during the plume evolution, i.e. day, night, morning and evening. Morning corresponds to those runs having the solar elevation angle negative at the emission and positive at the end of the run. For evening, the solar elevation angle has to be positive at the emission and negative at the end of the run.

We found that the multiple linear regressions explains the variance (R^2) in the fraction of NO_x remaining by 0.83, 0.88, 0.84 and 0.82 for day, night, morning and evening respectively. For the integrated ozone production efficiency (OPE) we found R^2 values of 0.82, 0.71 and 0.85 for day, morning and evening respectively. For night time the integrated OPE equals zero, as there is no photochemical ozone production during the night. These R^2 values give confidence in the fact that the equations are able to predict the fraction of NO_x remaining and integrate OPE in a global model, however, they require equations with many crossterms. We found that for the fraction of NO_x remaining in the morning the O_3 concentrations * temperature ($[\text{O}_3]*T$) is the most important variable, for day it was the pressure, for evening and night both again the $[\text{O}_3]*T$. The positive temperature*pressure relationship that we found to be important for daytime is hypothesized to reflect high temperature and pressure indicating 'fair' weather with associated high OH concentrations, and active chemistry, resulting in low fractions of NO_x remaining. The positive O_3 concentrations * temperature relationship that we found to be important for nighttime could reflect the fact that high O_3 concentrations influence the loss of NO_2 to NO_3 via [R6] and that high temperatures even further increase the loss of NO_2 to NO_3 and ultimately to HNO_3 . For the integrated OPE we found that in the morning the O_3 concentration is the most important variable, for day the temperature and for the evening the pressure.

Using this parametrization in global Chemistry Transport Models, e.g. GEOS-Chem, is anticipated to lead to better modeling of ship emissions and could prevent the over estimation of NO_x remaining that is now present in these models. Furthermore, as this parametrization is a simple formula it is easy portable between different models.

Further research can be done on the chemistry of the PARANOX model. The model now uses reaction rates from 1994, most of which now have updated values available in the literature. Evans and Jacob [2005] for example show that a new parametrization for the reaction probability of N_2O_5 on sulfate aerosols results in increase in NO_x , O_3 and OH concentrations, in better agreement with climatological observations.

The next step in improving the model studies of the ship emissions would be to improve the emissions inventories currently used, because these could also be one of the reasons for the observed difference in the ship O_3 production [Kasibhatla et al., 2000]. For this we can use satellite based observations of NO_2 , as these allow global monitoring in long time series and quantification of NO_x sources (e.g. Vinken [2008] and Boersma et al. [2007]). By comparing the modeled NO_2 column and the observed NO_2 column we can use the satellite observations to constrain the emissions.

A Chemistry Reactions

Species:

1	O3	2	OH	3	NO2
4	NO	5	H2O2	6	HO2NO2
7	HO2	8	HNO3	9	HCHO
10	CO	11	CH3CHO	12	CH3O2
13	CH3COC2H5	14	CH3COO2	15	C2H5O2
16	CH3COCOCH3	17	CH3COCHO	18	HCOCHO
19	NO3	20	N2O5	21	CH3OOH
22	CH4	23	C2H6	24	PAN
25	NC4H10	26	SC4H9O2	27	CH3COCHO2CH3
28	C2H4	29	CH2O2CH2OH	30	C3H6
31	CH3CHO2CH2OH	32	C2O _{rg} N	33	C3O _{rg} N
34	CH3OH	35	C5H8	36	C5O _{rg} N
37	C8H10	38	C6H4CH3CH2O2	39	OXYL1
40	CH3COCHCHCHO	41	CH3COCHOHCHO2CHO	42	OC5H8O2
43	CH3COCHCH2	44	OHCH3COCHCH2O2	45	HNO2

Reactions:

j1 : O3 + hv --> x3 OH + x4 O3 + O2
j3 : NO2 + hv --> NO + O3
j4a : H2O2 + hv --> 2OH
j4b : HO2NO2 + hv --> HO2 + NO2
j5 : HNO3 + hv --> NO2 + OH
j6 : HCHO + hv --> CO + 2HO2
j7 : HCHO + hv --> h2 + CO
j8 : CH3CHO + hv --> CH3O2 + HO2 + CO
j9 : CH3COC2H5 + hv --> CH3COO2 + C2H5O2
j10 : CH3COCOCH3 + hv --> 2CH3COO2
j11 : CH3COCHO + hv --> CO + CH3CHO
j12 : HCOCHO + hv --> HCHO + CO
j13 : NO3 + hv --> NO2 + O3
j14 : NO3 + hv --> NO + O2
j15 : N2O5 + hv --> NO2 + NO3
j16 : CH3OOH + hv --> HCHO + HO2 + OH
j17 : HNO2 + hv --> OH + NO
11 : O3 + NO --> NO2 + O2
12 : O3 + NO2 --> NO3 + O2
13 : O3 + OH --> HO2 + O2
14 : O3 + HO2 --> OH + 2O2
15 : NO + NO3 --> 2NO2
17 : NO + HO2 --> NO2 + OH
19 : NO2 + NO3 --> NO + NO2 + O2
20 : NO2 + NO3 + m --> N2O5 + m
21 : NO2 + OH + m --> HNO3 + m
22 : NO2 + HO2 --> HO2NO2
23 : HO2NO2 --> NO2 + HO2
24 : OH + HO2NO2 --> NO2 + H2O
29 : N2O5 --> NO2 + NO3
30 : OH + HO2 --> H2O + O2
31 : OH + H2O2 --> HO2 + H2O
33 : OH + h2 --> HO2 + H2O
35 : OH + HNO3 --> NO3 + H2O
36 : HO2 + HO2 --> H2O2 + O2

39 : OH + SO + m --> H2SO4 + m
42 : N2O5 + H2O --> 2HNO3
59 : OH + CH4 --> H2O + CH3O2
60 : CH3O2 + NO --> HCHO + HO2 + NO2
61 : CH3O2 + CH3O2 --> 2HCHO + 2HO2 + O2
62 : CH3O2 + CH3O2 --> 2HCHO + HO2 + H2O
63 : HO2 + CH3COO2 --> CH3OOH + 0.25 O3
65 : HO2 + CH3O2 --> CH3OOH + O2
66 : OH + HCHO --> H2O + HO2 + CO
67 : NO3 + HCHO --> HNO3 + HO2 + CO
70 : OH + CO --> HO2 + CO2
71 : C2H6 + OH --> C2H5O2 + H2O
72 : C2H5O2 + NO --> CH3CHO + HO2 + NO2
73 : C2H5O2 + CH3O2 --> CH3CHO + HCHO + 2HO2
75 : OH + CH3CHO --> H2O + CH3COO2
76 : OH + PAN --> HCHO + NO2
77 : CH3COO2 + NO2 + m --> PAN + m
78 : PAN + m --> CH3COO2 + NO2 + m
79 : CH3COO2 + NO --> CH3O2 + CO2 + NO2
80 : CH3O2 + CH3COO2 --> HCHO + HO2 + CH3O2 + CO2
81 : NC4H10 + OH --> SC4H9O2 + H2O
83 : SC4H9O2 + NO --> NO2 + x1 HO2 + x1 CH3COC2H5 + x2 CH3CHO +
x2 C2H5O2
84 : SC4H9O2 + CH3O2 --> x1 HO2 + x1 CH3COC2H5 + x2 CH3CHO +
x2 C2H5O2 + HO2
86 : CH3COC2H5 + OH --> CH3COCHO2CH3 + H2O
90 : C2H5O2 + C2H5O2 --> 2CH3CHO + 2HO2 + O2
91 : CH3COO2 + CH3COO2 --> 2CH3O2 + 2CO2 + O2
105 : CH3COCHO2CH3 + NO --> CH3COCOCH3 + HO2 + NO2
106 : CH3COCHO2CH3 + CH3O2 --> HCHO + HO2 + CH3COCOCH3
109 : C2H4 + OH + m --> CH2O2CH2OH + m
110 : CH2O2CH2OH + NO --> 2HCHO + HO2 + NO2
111 : CH2O2CH2OH + CH3O2 --> 3HCHO + 2HO2
112 : C2H4 + O3 --> HCHO + 0.42CO + 0.12HO2 + 0.12h2
123 : C3H6 + O3 --> 1.05HCHO + 0.12CH4 + 0.24CO + 0.34HO2 + 0.19OH +
0.43 CH3O2
124 : C3H6 + O3 --> CH3CHO + 0.42CO + 0.12HO2 + 0.12h2
125 : C3H6 + OH --> CH3CHO2CH2OH
126 : CH3CHO2CH2OH + NO --> CH3CHO + HCHO + HO2 + NO2
127 : CH3CHO2CH2OH + CH3O2 --> CH3CHO + 2HCHO + 2HO2
200 : CH4 + NO3 --> CH3O2 + HNO3
201 : C2H6 + NO3 --> C2H5O2 + HNO3
202 : NC4H10 + NO3 --> SC4H9O2 + HNO3
203 : C2H4 + NO3 --> C2OrgN
204 : C2OrgN + NO --> OrgN + H2O + NO2 - HO2
205 : C3H6 + NO3 --> C3OrgN
206 : C3OrgN + NO --> OrgN + NO2
207 : CH3OH + NO3 --> HCHO + HO2 + HNO3
208 : CH3CHO + NO3 --> CH3COO2 + HNO3
209 : C5H8 + NO3 --> C5OrgN
210 : C5OrgN + NO --> OrgN + NO2
211 : C8H10 + NO3 --> C6H4CH3CH2O2 + HNO3
212 : C6H4CH3CH2O2 + NO --> OrgN
221 : HCOCHO + OH --> HO2 + 2CO + H2O
222 : CH3COCHO --> CH3COO2 + CO + H2O
230 : C8H10 + OH --> OXYL1
231 : OXYL1 + NO --> CH3COCHO + CH3COCHCHCHO + HO2 + NO2
232 : CH3COCHCHCHO + OH --> CH3COCHOHCHO2CHO

233 : CH3COCHOHCHO2CHO + NO --> CH3COCHO + HCOCHO + HO2 + NO2
251 : C5H8 + OH --> OC5H8O2
252 : OC5H8O2 + NO --> CH3COCHCH2 + HCHO + NO2
253 : CH3COCHCH2 + OH --> OHCH3COCHCH2O2
254 : OHCH3COCHCH2O2 + NO --> CH3COCHO + HCHO + HO2 + NO2
nh1 : N2O5 + H2O(sulfate aerosol) --> 2HNO3
255 : HNO2 + OH --> NO2 + H2O
256 : NO + OH + m --> HNO2 + m

B Regression Coefficients

B.1 Fraction of NO_x remaining

B.1.1 Daytime

The daytime fraction of NO_x remaining regression coefficients A_i are given in Table 5.

B.1.2 Nighttime

The nighttime fraction of NO_x remaining regression coefficients B_i are given in Table 6.

Table 6: Regression coefficients of the regression on the fraction of NO_x remaining for nighttime.

		Estimate	Std. Error
B0	(Intercept)	-1.21E-01	2.01E-01
B1	Windspeed	2.09E-01	1.42E-02
B2	Temp	3.75E-03	6.87E-04
B4	ca.O3..E8	2.68E-04	1.59E-05
B5	Solar.Elevation.Angle.5.hrs.ago	-9.07E-03	1.90E-03
B6	Solar.Elevation.Angle	-7.38E-03	2.18E-03
B7	Emis.g.s.	-1.65E-03	5.91E-04
B9	ca.CO..E13	-2.00E+00	2.95E-01
B11	BLH	-5.46E-01	1.08E-01
B1,2	Windspeed*Temp	-7.57E-04	4.68E-05
B1,4	Windspeed*ca.O3..E8	1.07E-06	1.74E-07
B1,5	Windspeed*Solar.Elevation.Angle.5.hrs.ago	5.74E-05	1.55E-05
B1,7	Windspeed*Emis.g.s.	-7.81E-05	4.39E-06
B1,9	Windspeed*ca.CO..E13	-6.49E-02	4.98E-03
B1,11	Windspeed*BLH	8.18E-03	8.75E-04
B2,4	Temp*ca.O3..E8	-1.08E-06	5.53E-08
B2,5	Temp*Solar.Elevation.Angle.5.hrs.ago	2.97E-05	6.37E-06
B2,6	Temp*Solar.Elevation.Angle	2.62E-05	7.19E-06
B2,7	Temp*Emis.g.s.	8.00E-06	1.93E-06
B2,9	Temp*ca.CO..E13	7.40E-03	1.03E-03
B2,11	Temp*BLH	1.43E-03	3.52E-04
B4,5	ca.O3..E8*Solar.Elevation.Angle.5.hrs.ago	1.97E-07	1.80E-08
B4,7	ca.O3..E8*Emis.g.s.	6.01E-08	4.86E-09
B4,11	ca.O3..E8*BLH	5.34E-06	1.24E-06
B5,7	Solar.Elevation.Angle.5.hrs.ago*Emis.g.s.	-2.56E-06	4.88E-07
B5,11	Solar.Elevation.Angle.5.hrs.ago*BLH	-8.76E-04	1.22E-04
B6,9	Solar.Elevation.Angle*ca.CO..E13	-7.49E-04	2.75E-04
B6,11	Solar.Elevation.Angle*BLH	-4.40E-04	1.24E-04
B7,9	Emis.g.s.*ca.CO..E13	5.73E-04	1.03E-04
B7,11	Emis.g.s.*BLH	-3.56E-04	3.76E-05

B.1.3 Morning

The morning fraction of NO_x remaining regression coefficients C_i are given in Table 7.

B.1.4 Evening

The evening fraction of NO_x remaining regression coefficients D_i are given in Table 8.

Table 5: Regression coefficients of the regression on the fraction of NO_x remaining for daytime.

		Estimate	Std. Error
A0	(Intercept)	-1.98E+01	4.49E+00
A1	Windspeed	2.50E-01	4.39E-02
A2	Temp	6.36E-02	1.51E-02
A3	J.NO2.	7.49E+01	3.80E+01
A4	ca.O3..E8	2.25E-04	5.26E-05
A6	Solar.Elevation.Angle	-4.95E-02	2.97E-03
A8	JO1D.JNO2	5.51E+02	1.39E+02
A9	ca.CO..E13	-2.14E+00	1.04E+00
A10	Pressure	2.47E-04	4.44E-05
A1,2	Windspeed*Temp	-5.65E-04	7.38E-05
A1,3	Windspeed*J.NO2.	-1.42E+00	2.87E-01
A1,5	Windspeed*Solar.Elevation.Angle.5.hrs.ago	-2.39E-04	2.18E-05
A1,6	Windspeed*Solar.Elevation.Angle	-1.30E-04	2.40E-05
A1,7	Windspeed*Emis.g.s.	-1.26E-04	5.56E-06
A1,8	Windspeed*JO1D.JNO2	4.40E+00	7.87E-01
A1,9	Windspeed*ca.CO..E13	1.64E-02	5.91E-03
A1,10	Windspeed*Pressure	-1.01E-06	3.96E-07
A1,11	Windspeed*BLH	1.41E-02	1.12E-03
A2,3	Temp*J.NO2.	-3.59E-01	1.32E-01
A2,4	Temp*ca.O3..E8	-4.09E-07	8.62E-08
A2,6	Temp*Solar.Elevation.Angle	1.84E-04	9.92E-06
A2,7	Temp*Emis.g.s.	6.41E-06	2.65E-06
A2,10	Temp*Pressure	-7.77E-07	1.50E-07
A2,11	Temp*BLH	3.63E-03	4.87E-04
A3,4	J.NO2.*ca.O3..E8	1.25E-03	1.71E-04
A3,5	J.NO2.*Solar.Elevation.Angle.5.hrs.ago	-1.35E-01	4.83E-02
A3,6	J.NO2.*Solar.Elevation.Angle	5.36E-01	4.89E-02
A3,7	J.NO2.*Emis.g.s.	1.84E-02	4.59E-03
A3,8	J.NO2.*JO1D.JNO2	-5.91E+03	5.58E+02
A3,9	J.NO2.*ca.CO..E13	2.46E+01	9.83E+00
A3,11	J.NO2.*BLH	4.41E+00	1.01E+00
A4,5	ca.O3..E8*Solar.Elevation.Angle.5.hrs.ago	-9.98E-08	2.88E-08
A4,6	ca.O3..E8*Solar.Elevation.Angle	-3.64E-07	3.09E-08
A4,7	ca.O3..E8*Emis.g.s.	3.83E-08	6.64E-09
A4,9	ca.O3..E8*ca.CO..E13	4.03E-05	4.53E-06
A4,10	ca.O3..E8*Pressure	-1.41E-09	4.09E-10
A4,11	ca.O3..E8*BLH	7.86E-06	1.38E-06
A5,7	Solar.Elevation.Angle.5.hrs.ago*Emis.g.s.	3.20E-06	9.03E-07
A5,8	Solar.Elevation.Angle.5.hrs.ago*JO1D.JNO2	-3.31E-01	1.15E-01
A5,9	Solar.Elevation.Angle.5.hrs.ago*ca.CO..E13	-2.38E-03	6.93E-04
A6,7	Solar.Elevation.Angle*Emis.g.s.	-3.72E-06	9.21E-07
A6,8	Solar.Elevation.Angle*JO1D.JNO2	-7.85E-01	1.28E-01
A6,9	Solar.Elevation.Angle*ca.CO..E13	-4.90E-03	7.81E-04
A7,9	Emis.g.s.*ca.CO..E13	-1.12E-03	2.02E-04
A7,11	Emis.g.s.*BLH	-2.55E-04	4.73E-05
A8,10	JO1D.JNO2*Pressure	-3.66E-03	8.00E-04
A9,10	ca.CO..E13*Pressure	2.05E-05	1.05E-05
A10,11	Pressure*BLH	-7.65E-06	3.27E-06

Table 7: Regression coefficients of the regression on the fraction of NO_x remaining for morning.

		Estimate	Std. Error
C0	(Intercept)	9.15E-01	2.64E-01
C1	Windspeed	1.22E-01	2.22E-02
C3	J.NO2.	1.03E+02	4.95E+01
C4	ca.O3..E8	1.34E-04	2.47E-05
C6	Solar.Elevation.Angle	2.47E-03	7.40E-04
C7	Emis.g.s.	-4.43E-03	7.06E-04
C11	BLH	-1.03E-01	1.58E-02
C1,2	Windspeed*Temp	-4.77E-04	7.83E-05
C1,4	Windspeed*ca.O3..E8	5.19E-07	1.80E-07
C1,5	Windspeed*Solar.Elevation.Angle.5.hrs.ago	9.96E-05	3.67E-05
C1,7	Windspeed*Emis.g.s.	-1.02E-04	5.64E-06
C1,8	Windspeed*JO1D.JNO2	-2.36E+00	6.43E-01
C1,11	Windspeed*BLH	1.14E-02	1.09E-03
C2,4	Temp*ca.O3..E8	-6.17E-07	8.76E-08
C2,7	Temp*Emis.g.s.	1.91E-05	2.36E-06
C2,8	Temp*JO1D.JNO2	-1.25E+00	5.55E-01
C3,6	J.NO2.*Solar.Elevation.Angle	-5.74E-01	1.26E-01
C3,8	J.NO2.*JO1D.JNO2	-6.33E+03	1.41E+03
C4,5	ca.O3..E8*Solar.Elevation.Angle.5.hrs.ago	1.77E-07	4.21E-08
C4,7	ca.O3..E8*Emis.g.s.	4.11E-08	5.91E-09
C4,8	ca.O3..E8*JO1D.JNO2	3.52E-03	9.55E-04
C5,6	Solar.Elevation.Angle.5.hrs.ago*Solar.Elevation.Angle	7.44E-05	1.34E-05
C5,7	Solar.Elevation.Angle.5.hrs.ago*Emis.g.s.	3.85E-06	9.04E-07
C5,8	Solar.Elevation.Angle.5.hrs.ago*JO1D.JNO2	-3.48E+00	3.43E-01
C5,11	Solar.Elevation.Angle.5.hrs.ago*BLH	-5.17E-04	2.48E-04
C6,8	Solar.Elevation.Angle*JO1D.JNO2	1.77E+00	3.39E-01
C7,11	Emis.g.s.*BLH	-1.93E-04	4.59E-05

Table 8: Regression coefficients of the regression on the fraction of NO_x remaining for evening.

		Estimate	Std. Error
D1	Windspeed	6.08E-02	1.65E-02
D2	Temp	2.84E-03	8.64E-04
D3	J.NO2.	2.87E+02	9.07E+01
D4	ca.O3..E8	1.92E-04	1.92E-05
D5	Solar.Elevation.Angle.5.hrs.ago	7.76E-02	2.88E-03
D7	Emis.g.s.	-5.80E-03	7.91E-04
D8	JO1D.JNO2	-4.11E+03	1.17E+03
D11	BLH	-4.50E-02	1.23E-02
D1,2	Windspeed*Temp	-2.16E-04	5.84E-05
D1,3	Windspeed*J.NO2.	-7.94E+00	3.56E+00
D1,4	Windspeed*ca.O3..E8	9.08E-07	1.55E-07
D1,5	Windspeed*Solar.Elevation.Angle.5.hrs.ago	-5.12E-04	3.69E-05
D1,6	Windspeed*Solar.Elevation.Angle	2.93E-04	3.61E-05
D1,7	Windspeed*Emis.g.s.	-5.75E-05	4.56E-06
D1,11	Windspeed*BLH	4.93E-03	8.27E-04
D2,4	Temp*ca.O3..E8	-7.91E-07	7.03E-08
D2,5	Temp*Solar.Elevation.Angle.5.hrs.ago	-2.71E-04	9.48E-06
D2,7	Temp*Emis.g.s.	2.20E-05	2.83E-06
D2,8	Temp*JO1D.JNO2	1.48E+01	4.27E+00
D2,9	Temp*ca.CO..E13	2.65E-03	1.27E-03
D3,4	J.NO2.*ca.O3..E8	-1.84E-02	6.80E-03
D3,6	J.NO2.*Solar.Elevation.Angle	3.11E+01	1.31E+01
D3,8	J.NO2.*JO1D.JNO2	-8.75E+05	2.17E+05
D3,9	J.NO2.*ca.CO..E13	6.59E+02	1.73E+02
D4,5	ca.O3..E8*Solar.Elevation.Angle.5.hrs.ago	1.67E-07	4.34E-08
D4,6	ca.O3..E8*Solar.Elevation.Angle	2.36E-07	4.49E-08
D4,7	ca.O3..E8*Emis.g.s.	3.79E-08	5.46E-09
D4,11	ca.O3..E8*BLH	2.53E-06	1.06E-06
D5,6	Solar.Elevation.Angle.5.hrs.ago*Solar.Elevation.Angle	-9.83E-05	3.99E-06
D5,7	Solar.Elevation.Angle.5.hrs.ago*Emis.g.s.	7.87E-06	1.78E-06
D5,8	Solar.Elevation.Angle.5.hrs.ago*JO1D.JNO2	-6.84E+00	2.23E+00
D5,9	Solar.Elevation.Angle.5.hrs.ago*ca.CO..E13	-2.11E-03	7.53E-04
D5,11	Solar.Elevation.Angle.5.hrs.ago*BLH	-8.64E-04	1.71E-04
D6,7	Solar.Elevation.Angle*Emis.g.s.	5.81E-06	1.85E-06
D6,8	Solar.Elevation.Angle*JO1D.JNO2	-2.96E+01	1.11E+01
D7,9	Emis.g.s.*ca.CO..E13	-3.69E-04	1.51E-04
D8,11	JO1D.JNO2*BLH	1.03E+02	4.14E+01

B.2 Integrated OPE

B.2.1 Daytime

The daytime integrated OPE regression coefficients E_i are given in Table 9.

B.2.2 Morning

The morning integrated OPE regression coefficients F_i are given in Table 10.

Table 10: Regression coefficients of the regression on the integrated OPE for morning.

		Estimate	Std. Error
F0	(Intercept)	-6.87E+00	1.96E+01
F3	J.NO2.	1.46E+03	2.62E+02
F4	ca.O3..E8	-1.11E-02	1.69E-03
F6	Solar.Elevation.Angle	3.67E+00	6.53E-01
F7	Emis.g.s.	-2.29E-02	3.82E-03
F8	JO1D.JNO2	-5.40E+04	1.04E+04
F9	ca.CO..E13	1.48E+02	3.57E+01
F11	BLH	3.06E+01	1.20E+01
F1,3	Windspeed*J.NO2.	-2.89E+01	1.29E+01
F1,5	Windspeed*Solar.Elevation.Angle.5.hrs.ago	2.48E-03	1.24E-03
F1,8	Windspeed*JO1D.JNO2	2.28E+02	3.36E+01
F3,4	J.NO2.*ca.O3..E8	-2.19E-01	1.72E-02
F3,5	J.NO2.*Solar.Elevation.Angle.5.hrs.ago	2.82E+01	3.68E+00
F3,6	J.NO2.*Solar.Elevation.Angle	-1.36E+01	4.45E+00
F3,9	J.NO2.*ca.CO..E13	6.87E+03	3.94E+02
F3,11	J.NO2.*BLH	4.25E+02	1.12E+02
F4,5	ca.O3..E8*Solar.Elevation.Angle.5.hrs.ago	-1.07E-05	1.97E-06
F4,6	ca.O3..E8*Solar.Elevation.Angle	1.06E-05	3.29E-06
F4,7	ca.O3..E8*Emis.g.s.	3.75E-06	2.67E-07
F4,8	ca.O3..E8*JO1D.JNO2	1.16E-01	4.58E-02
F4,9	ca.O3..E8*ca.CO..E13	-2.34E-03	1.30E-04
F4,10	ca.O3..E8*Pressure	1.09E-07	1.66E-08
F5,7	Solar.Elevation.Angle.5.hrs.ago*Emis.g.s.	-2.23E-04	5.44E-05
F5,8	Solar.Elevation.Angle.5.hrs.ago*JO1D.JNO2	-3.70E+01	1.12E+01
F5,10	Solar.Elevation.Angle.5.hrs.ago*ca.CO..E13	1.93E-01	3.33E-02
F6,10	Solar.Elevation.Angle*Pressure	-3.71E-05	6.45E-06
F7,10	Emis.g.s.*ca.CO..E13	-7.18E-02	6.68E-03
F8,9	JO1D.JNO2*ca.CO..E13	-1.36E+04	9.51E+02
F8,10	JO1D.JNO2*Pressure	5.42E-01	1.03E-01
F8,11	JO1D.JNO2*BLH	-9.68E+02	3.05E+02
F9,10	ca.CO..E13*Pressure	-1.12E-03	3.58E-04
F9,11	ca.CO..E13*BLH	-9.11E+00	1.90E+00
F10,11	Pressure*BLH	-2.86E-04	1.18E-04

B.2.3 Evening

The evening integrated OPE regression coefficients G_i are given in Table 11.

Table 9: Regression coefficients of the regression on the integrated OPE for daytime.

		Estimate	Std. Error
E0	(Intercept)	-1.86E+01	1.24E+01
E1	Windspeed	3.30E+00	4.78E-01
E2	Temp	3.25E-01	2.35E-02
E3	J.NO2.	1.06E+04	1.75E+03
E4	ca.O3..E8	-6.85E-03	1.34E-03
E5	Solar.Elevation.Angle.5.hrs.ago	8.43E-01	6.03E-02
E6	Solar.Elevation.Angle	-3.33E-01	1.20E-01
E7	Emis.g.s.	-1.68E-01	3.75E-02
E9	ca.CO..E13	1.92E+02	2.96E+01
E10	Pressure	-7.66E-04	1.01E-04
E1,2	Windspeed*Temp	-1.02E-02	1.64E-03
E1,3	Windspeed*J.NO2.	3.70E+01	6.52E+00
E1,4	Windspeed*ca.O3..E8	-4.45E-05	5.21E-06
E1,6	Windspeed*Solar.Elevation.Angle	-3.69E-03	5.77E-04
E1,6	Windspeed*Solar.Elevation.Angle.5.hrs.ago	3.09E-03	5.30E-04
E1,8	Windspeed*JO1D.JNO2	4.73E+01	1.84E+01
E1,9	Windspeed*ca.CO..E13	9.83E-01	1.34E-01
E2,3	Temp*J.NO2.	-1.41E+01	2.90E+00
E2,4	Temp*ca.O3..E8	-1.28E-05	2.44E-06
E2,5	Temp*Solar.Elevation.Angle.5.hrs.ago	-2.66E-03	2.03E-04
E2,7	Temp*Emis.g.s.	7.25E-04	5.78E-05
E2,11	Temp*BLH	-1.13E-01	1.23E-02
E3,4	J.NO2.*ca.O3..E8	-5.66E-02	8.43E-03
E3,5	J.NO2.*Solar.Elevation.Angle.5.hrs.ago	-1.37E+01	7.95E-01
E3,7	J.NO2.*Emis.g.s.	-1.41E+00	1.06E-01
E3,8	J.NO2.*JO1D.JNO2	-1.73E+05	1.30E+04
E3,9	J.NO2.*ca.CO..E13	2.51E+03	2.53E+02
E3,10	J.NO2.*Pressure	-5.41E-02	1.50E-02
E4,5	ca.O3..E8*Solar.Elevation.Angle.5.hrs.ago	1.37E-06	6.84E-07
E4,6	ca.O3..E8*Solar.Elevation.Angle	8.25E-06	7.52E-07
E4,7	ca.O3..E8*Emis.g.s.	4.07E-06	1.53E-07
E4,8	ca.O3..E8*JO1D.JNO2	-7.21E-02	2.24E-02
E4,9	ca.O3..E8*ca.CO..E13	-2.18E-03	1.10E-04
E4,10	ca.O3..E8*Pressure	1.04E-07	1.01E-08
E4,11	ca.O3..E8*BLH	-2.58E-04	3.87E-05
E5,6	Solar.Elevation.Angle.5.hrs.ago*Solar.Elevation.Angle	1.07E-03	1.33E-04
E5,9	Solar.Elevation.Angle.5.hrs.ago*ca.CO..E13	-1.78E-01	2.01E-02
E5,11	Solar.Elevation.Angle.5.hrs.ago*BLH	1.33E-02	4.17E-03
E6,7	Solar.Elevation.Angle*Emis.g.s.	1.46E-04	1.60E-05
E6,8	Solar.Elevation.Angle*JO1D.JNO2	2.03E+01	1.41E+00
E6,9	Solar.Elevation.Angle*ca.CO..E13	-2.44E-01	2.23E-02
E6,10	Solar.Elevation.Angle*Pressure	2.42E-06	1.18E-06
E7,9	Emis.g.s.*ca.CO..E13	-9.39E-02	4.83E-03
E7,10	Emis.g.s.*Pressure	-7.28E-07	2.94E-07
E7,11	Emis.g.s.*BLH	3.83E-03	1.07E-03
E8,9	JO1D.JNO2*ca.CO..E13	-3.91E+03	6.11E+02
E8,10	JO1D.JNO2*Pressure	1.11E-01	4.11E-02
E9,10	ca.CO..E13*BLH	7.35E+00	1.28E+00
E9,10	ca.CO..E13*Pressure	-1.23E-03	2.46E-04
E10,11	Pressure*BLH	4.10E-04	6.38E-05

Table 11: Regression coefficients of the regression on the integrated OPE for evening.

		Estimate	Std. Error
G0	(Intercept)	2.95E+01	1.01E+01
G5	Solar.Elevation.Angle.5.hrs.ago	4.57E-01	1.14E-01
G8	JO1D.JNO2	8.61E+04	2.71E+04
G9	ca.CO..E13	-6.39E+01	1.71E+01
G10	Pressure	-2.75E-04	8.49E-05
G11	BLH	-2.58E+01	5.73E+00
G1,2	Windspeed*Temp	8.98E-03	1.29E-03
G1,4	Windspeed*ca.O3..E8	-1.98E-05	4.07E-06
G1,5	Windspeed*Solar.Elevation.Angle.5.hrs.ago	5.29E-03	7.89E-04
G1,6	Windspeed*Solar.Elevation.Angle	5.24E-03	7.73E-04
G1,7	Windspeed*Emis.g.s.	-7.41E-04	9.66E-05
G1,9	Windspeed*ca.CO..E13	5.58E-01	1.26E-01
G1,10	Windspeed*Pressure	-1.86E-05	6.81E-06
G1,11	Windspeed*BLH	9.14E-02	1.86E-02
G2,4	Temp*ca.O3..E8	-5.83E-06	1.44E-06
G2,6	Temp*Solar.Elevation.Angle	-5.34E-04	1.95E-04
G2,7	Temp*Emis.g.s.	1.62E-04	6.01E-05
G2,8	Temp*JO1D.JNO2	-2.28E+02	9.48E+01
G2,9	Temp*ca.CO..E13	1.23E-01	2.96E-02
G3,4	J.NO2.*ca.O3..E8	9.78E-01	2.06E-01
G3,9	J.NO2.*ca.CO..E13	-1.92E+04	5.72E+03
G4,5	ca.O3..E8*Solar.Elevation.Angle.5.hrs.ago	-7.74E-06	5.14E-07
G4,7	ca.O3..E8*Emis.g.s.	1.37E-06	1.19E-07
G4,8	ca.O3..E8*JO1D.JNO2	-1.42E+00	2.96E-01
G4,9	ca.O3..E8*ca.CO..E13	-6.19E-04	7.10E-05
G4,10	ca.O3..E8*Pressure	2.65E-08	7.14E-09
G4,11	ca.O3..E8*BLH	-6.34E-05	2.25E-05
G5,6	Solar.Elevation.Angle.5.hrs.ago*Solar.Elevation.Angle	1.74E-03	8.31E-05
G5,7	Solar.Elevation.Angle.5.hrs.ago*Emis.g.s.	-3.36E-04	3.71E-05
G5,8	Solar.Elevation.Angle.5.hrs.ago*JO1D.JNO2	-2.86E+02	4.77E+01
G5,10	Solar.Elevation.Angle.5.hrs.ago*Pressure	-2.78E-06	1.12E-06
G5,11	Solar.Elevation.Angle.5.hrs.ago*BLH	2.12E-02	5.14E-03
G6,9	Solar.Elevation.Angle*ca.CO..E13	1.09E-01	1.36E-02
G6,11	Solar.Elevation.Angle*BLH	1.14E-02	4.76E-03
G7,9	Emis.g.s.*ca.CO..E13	-1.56E-02	3.98E-03
G7,10	Emis.g.s.*Pressure	-7.08E-07	2.29E-07
G9,10	ca.CO..E13*Pressure	4.03E-04	1.82E-04
G10,11	Pressure*BLH	2.60E-04	5.65E-05

C Statistical output from regressions

C.1 Fraction of NO_x remaning

C.1.1 Daytime

The statistical output for the regression coefficients of the fraction of NO_x remaining for daytime are given in Table 12.

The residual standard error was 0.092 on 7502 degrees of freedom.

Multiple R-Squared: 0.83, Adjusted R-squared: 0.83.

F-statistic: 681 on 53 and 7502 DF, p-value: < 2.2e-16.

Residuals; Min: -0.374, 1Q: -0.054, Median: -0.007, 3Q: 0.041, Max: 0.662

C.1.2 Nighttime

The statistical output for the regression coefficients of the fraction of NO_x remaining for nighttime are given in Table 13.

The residual standard error: 0.054 on 4264 degrees of freedom.

Multiple R-Squared: 0.88, Adjusted R-squared: 0.88.

F-statistic: 969.1 on 33 and 4264 DF, p-value: < 2.2e-16.

Residuals; Min: -0.391, 1Q: -0.0199, Median: -0.000, 3Q: 0.022, Max: 0.352

C.1.3 Morning

The statistical output for the regression coefficients of the fraction of NO_x remaining for morning are given in Table 14.

The residual standard error was 0.065 on 3628 degrees of freedom.

Multiple R-Squared: 0.84, Adjusted R-squared: 0.84.

F-statistic: 587.4 on 33 and 3628 DF, p-value: < 2.2e-16.

Residuals; Min: -0.440, 1Q: -0.032, Median: -0.003, 3Q: 0.028, Max: 0.830

C.1.4 Evening

The statistical output for the regression coefficients of the fraction of NO_x remaining for evening are given in Table 15.

The residual standard error was 0.063 on 4262 degrees of freedom.

Multiple R-Squared: 0.82, Adjusted R-squared: 0.82.

F-statistic: 482.6 on 40 and 4262 DF, p-value: < 2.2e-16.

Residuals; Min: -0.291, 1Q: -0.0330, Median: -0.004, 3Q: 0.0290, Max: 0.461

Table 12: Statistical output for the regression coefficients of the fraction of NO_x remaining for daytime.

		t value	Pr(> t)
A0	(Intercept)	-4.414	1.03E-05
A1	Windspeed	5.688	1.34E-08
A2	Temp	4.2	2.70E-05
A3	J.NO2.	1.975	0.048348
A4	ca.O3..E8	4.284	1.86E-05
A6	Solar.Elevation.Angle	-16.674	< 2e-16
A8	JO1D.JNO2	3.967	7.34E-05
A9	ca.CO..E13	-2.057	0.039702
A10	Pressure	5.566	2.69E-08
A1,11	Windspeed*BLH	12.581	< 2e-16
A1,2	Windspeed*Temp	-7.657	2.15E-14
A1,3	Windspeed*J.NO2.	-4.964	7.05E-07
A1,5	Windspeed*Solar.Elevation.Angle.5.hrs.ago	-10.974	< 2e-16
A1,6	Windspeed*Solar.Elevation.Angle	-5.415	6.32E-08
A1,7	Windspeed*Emis.g.s.	-22.645	< 2e-16
A1,8	Windspeed*JO1D.JNO2	5.589	2.36E-08
A1,9	Windspeed*ca.CO..E13	2.774	0.005553
A1,10	Windspeed*Pressure	-2.545	0.010936
A2,10	Temp*Pressure	-5.185	2.21E-07
A2,11	Temp*BLH	7.456	9.94E-14
A2,3	Temp*J.NO2.	-2.721	0.006527
A2,4	Temp*ca.O3..E8	-4.745	2.13E-06
A2,6	Temp*Solar.Elevation.Angle	18.545	< 2e-16
A2,7	Temp*Emis.g.s.	2.423	0.015431
A3,11	J.NO2.*BLH	4.388	1.16E-05
A3,4	J.NO2.*ca.O3..E8	7.343	2.30E-13
A3,5	J.NO2.*Solar.Elevation.Angle.5.hrs.ago	-2.8	0.005126
A3,6	J.NO2.*Solar.Elevation.Angle	10.953	< 2e-16
A3,7	J.NO2.*Emis.g.s.	3.995	6.52E-05
A3,8	J.NO2.*JO1D.JNO2	-10.594	< 2e-16
A3,9	J.NO2.*ca.CO..E13	2.506	0.012214
A4,10	ca.O3..E8*Pressure	-3.437	0.000591
A4,11	ca.O3..E8*BLH	5.711	1.17E-08
A4,5	ca.O3..E8*Solar.Elevation.Angle.5.hrs.ago	-3.471	0.000522
A4,6	ca.O3..E8*Solar.Elevation.Angle	-11.797	< 2e-16
A4,7	ca.O3..E8*Emis.g.s.	5.763	8.58E-09
A4,9	ca.O3..E8*ca.CO..E13	8.893	< 2e-16
A5,7	Solar.Elevation.Angle.5.hrs.ago*Emis.g.s.	3.545	0.000395
A5,8	Solar.Elevation.Angle.5.hrs.ago*JO1D.JNO2	-2.885	0.00392
A5,9	Solar.Elevation.Angle.5.hrs.ago*ca.CO..E13	-3.436	0.000593
A6,7	Solar.Elevation.Angle*Emis.g.s.	-4.033	5.56E-05
A6,8	Solar.Elevation.Angle*JO1D.JNO2	-6.111	1.04E-09
A6,9	Solar.Elevation.Angle*ca.CO..E13	-6.268	3.85E-10
A7,11	Emis.g.s.*BLH	-5.395	7.05E-08
A7,9	Emis.g.s.*ca.CO..E13	-5.512	3.66E-08
A8,10	JO1D.JNO2*Pressure	-4.578	4.78E-06
A9,10	ca.CO..E13*Pressure	1.963	0.049715
A10,11	Pressure*BLH	-2.34	0.019333

Table 13: Statistical output for the regression coefficients of the fraction of NO_x remaining for nighttime.

		t value	Pr(> t)
B0	(Intercept)	-0.599	0.549099
B1	Windspeed	14.721	< 2e-16
B2	Temp	5.455	5.17E-08
B4	ca.O3..E8	16.86	< 2e-16
B5	Solar.Elevation.Angle.5.hrs.ago	-4.775	1.86E-06
B6	Solar.Elevation.Angle	-3.386	0.000716
B7	Emis.g.s.	-2.795	0.005206
B9	ca.CO..E13	-6.767	1.50E-11
B11	BLH	-5.04	4.85E-07
B1,2	Windspeed*Temp	-16.169	< 2e-16
B1,4	Windspeed*ca.O3..E8	6.128	9.72E-10
B1,5	Windspeed*Solar.Elevation.Angle.5.hrs.ago	3.706	0.000214
B1,7	Windspeed*Emis.g.s.	-17.802	< 2e-16
B1,9	Windspeed*ca.CO..E13	-13.02	< 2e-16
B1,11	Windspeed*BLH	9.348	< 2e-16
B2,4	Temp*ca.O3..E8	-19.599	< 2e-16
B2,5	Temp*Solar.Elevation.Angle.5.hrs.ago	4.662	3.22E-06
B2,6	Temp*Solar.Elevation.Angle	3.643	0.000272
B2,7	Temp*Emis.g.s.	4.146	3.45E-05
B2,9	Temp*ca.CO..E13	7.213	6.45E-13
B2,11	Temp*BLH	4.052	5.17E-05
B4,5	ca.O3..E8*Solar.Elevation.Angle.5.hrs.ago	10.96	< 2e-16
B4,7	ca.O3..E8*Emis.g.s.	12.371	< 2e-16
B4,11	ca.O3..E8*BLH	4.304	1.71E-05
B5,7	Solar.Elevation.Angle.5.hrs.ago*Emis.g.s.	-5.259	1.52E-07
B5,11	Solar.Elevation.Angle.5.hrs.ago*BLH	-7.184	7.98E-13
B6,9	Solar.Elevation.Angle*ca.CO..E13	-2.721	0.006526
B6,11	Solar.Elevation.Angle*BLH	-3.549	0.000391
B7,9	Emis.g.s.*ca.CO..E13	5.569	2.72E-08
B7,11	Emis.g.s.*BLH	-9.449	< 2e-16

Table 14: Statistical output for the regression coefficients of the fraction of NO_x remaining for the morning.

		t value	Pr(> t)
C0	(Intercept)	3.466	0.000534
C1	Windspeed	5.488	4.35E-08
C3	J.NO2.	2.071	0.038426
C4	ca.O3..E8	5.433	5.91E-08
C6	Solar.Elevation.Angle	3.339	0.000849
C7	Emis.g.s.	-6.273	3.97E-10
C11	BLH	-6.496	9.36E-11
C1,2	Windspeed*Temp	-6.084	1.29E-09
C1,4	Windspeed*ca.O3..E8	2.885	0.003933
C1,5	Windspeed*Solar.Elevation.Angle.5.hrs.ago	2.714	0.006684
C1,7	Windspeed*Emis.g.s.	-18.158	< 2e-16
C1,8	Windspeed*JO1D.JNO2	-3.674	0.000242
C1,11	Windspeed*BLH	10.475	< 2e-16
C2,4	Temp*ca.O3..E8	-7.045	2.21E-12
C2,7	Temp*Emis.g.s.	8.061	1.02E-15
C2,8	Temp*JO1D.JNO2	-2.252	0.024387
C3,6	J.NO2.*Solar.Elevation.Angle	-4.572	4.99E-06
C3,8	J.NO2.*JO1D.JNO2	-4.503	6.91E-06
C4,5	ca.O3..E8*Solar.Elevation.Angle.5.hrs.ago	4.195	2.80E-05
C4,7	ca.O3..E8*Emis.g.s.	6.945	4.47E-12
C4,8	ca.O3..E8*JO1D.JNO2	3.681	0.000236
C5,6	Solar.Elevation.Angle.5.hrs.ago*Solar.Elevation.Angle	5.56	2.89E-08
C5,7	Solar.Elevation.Angle.5.hrs.ago*Emis.g.s.	4.264	2.06E-05
C5,8	Solar.Elevation.Angle.5.hrs.ago*JO1D.JNO2	-10.142	< 2e-16
C5,11	Solar.Elevation.Angle.5.hrs.ago*BLH	-2.089	0.036774
C6,8	Solar.Elevation.Angle*JO1D.JNO2	5.233	1.76E-07
C7,11	Emis.g.s.*BLH	-4.208	2.64E-05

Table 15: Statistical output for the regression coefficients of the fraction of NO_x remaining for the evening.

		t value	Pr(> t)
D1	Windspeed	3.697	0.000221
D2	Temp	3.283	0.001036
D3	J.NO2.	3.158	0.001602
D4	ca.O3..E8	10	< 2e-16
D5	Solar.Elevation.Angle.5.hrs.ago	27.001	< 2e-16
D7	Emis.g.s.	-7.326	2.82E-13
D8	JO1D.JNO2	-3.514	0.000447
D11	BLH	-3.662	0.000253
D1,2	Windspeed*Temp	-3.692	0.000225
D1,3	Windspeed*J.NO2.	-2.232	0.025644
D1,4	Windspeed*ca.O3..E8	5.854	5.16E-09
D1,5	Windspeed*Solar.Elevation.Angle.5.hrs.ago	-13.866	< 2e-16
D1,6	Windspeed*Solar.Elevation.Angle	8.124	5.84E-16
D1,7	Windspeed*Emis.g.s.	-12.606	< 2e-16
D1,11	Windspeed*BLH	5.965	2.64E-09
D2,4	Temp*ca.O3..E8	-11.247	< 2e-16
D2,5	Temp*Solar.Elevation.Angle.5.hrs.ago	-28.568	< 2e-16
D2,7	Temp*Emis.g.s.	7.784	8.79E-15
D2,8	Temp*JO1D.JNO2	3.462	0.000542
D2,9	Temp*ca.CO..E13	2.099	0.035916
D3,4	J.NO2.*ca.O3..E8	-2.701	0.006944
D3,6	J.NO2.*Solar.Elevation.Angle	2.38	0.017341
D3,8	J.NO2.*JO1D.JNO2	-4.041	5.41E-05
D3,9	J.NO2.*ca.CO..E13	3.806	0.000143
D4,5	ca.O3..E8*Solar.Elevation.Angle.5.hrs.ago	3.851	0.000119
D4,6	ca.O3..E8*Solar.Elevation.Angle	5.268	1.45E-07
D4,7	ca.O3..E8*Emis.g.s.	6.945	4.36E-12
D4,11	ca.O3..E8*BLH	2.388	0.016969
D5,6	Solar.Elevation.Angle.5.hrs.ago*Solar.Elevation.Angle	-24.627	< 2e-16
D5,7	Solar.Elevation.Angle.5.hrs.ago*Emis.g.s.	4.418	1.02E-05
D5,8	Solar.Elevation.Angle.5.hrs.ago*JO1D.JNO2	-3.063	0.002204
D5,9	Solar.Elevation.Angle.5.hrs.ago*ca.CO..E13	-2.799	0.005155
D5,11	Solar.Elevation.Angle.5.hrs.ago*BLH	-5.06	4.38E-07
D6,7	Solar.Elevation.Angle*Emis.g.s.	3.142	0.001689
D6,8	Solar.Elevation.Angle*JO1D.JNO2	-2.666	0.007714
D7,9	Emis.g.s.*ca.CO..E13	-2.438	0.014794
D8,11	JO1D.JNO2*BLH	2.495	0.01265

C.2 Integrated OPE

C.2.1 Daytime

The statistical output for the regression coefficients of the integrated OPE for daytime are given in Table 16.

The residual standard error was 2.11 on 7500 degrees of freedom.

Multiple R-Squared: 0.82, Adjusted R-squared: 0.81.

F-statistic: 604.4 on 55 and 7500 DF, p-value: < 2.2e-16.

Residuals; Min: -22.684, 1Q: -1.030, Median: -0.124, 3Q: 0.912, Max: 61.651

Table 16: Statistical output for the regression coefficients of integrated OPE for daytime.

		t value	Pr(> t)
E0	(Intercept)	-1.509	0.131448
E1	Windspeed	6.914	5.11E-12
E2	Temp	13.828	< 2e-16
E3	J.NO2.	6.032	1.70E-09
E4	ca.O3..E8	-5.096	3.56E-07
E5	Solar.Elevation.Angle.5.hrs.ago	13.989	< 2e-16
E6	Solar.Elevation.Angle	-2.783	0.005392
E7	Emis.g.s.	-4.481	7.52E-06
E9	ca.CO..E13	6.497	8.72E-11
E10	Pressure	-7.599	3.34E-14
E1,2	Windspeed*Temp	-6.248	4.40E-10
E1,3	Windspeed*J.NO2.	5.663	1.54E-08
E1,4	Windspeed*ca.O3..E8	-8.536	< 2e-16
E1,6	Windspeed*Solar.Elevation.Angle	-6.408	1.57E-10
E1,6	Windspeed*Solar.Elevation.Angle.5.hrs.ago	5.825	5.96E-09
E1,8	Windspeed*JO1D.JNO2	2.567	0.010281
E1,9	Windspeed*ca.CO..E13	7.352	2.17E-13
E2,3	Temp*J.NO2.	-4.848	1.27E-06
E2,4	Temp*ca.O3..E8	-5.238	1.67E-07
E2,5	Temp*Solar.Elevation.Angle.5.hrs.ago	-13.121	< 2e-16
E2,7	Temp*Emis.g.s.	12.54	< 2e-16
E2,11	Temp*BLH	-9.181	< 2e-16
E3,4	J.NO2.*ca.O3..E8	-6.715	2.01E-11
E3,5	J.NO2.*Solar.Elevation.Angle.5.hrs.ago	-17.188	< 2e-16
E3,7	J.NO2.*Emis.g.s.	-13.288	< 2e-16
E3,8	J.NO2.*JO1D.JNO2	-13.278	< 2e-16
E3,9	J.NO2.*ca.CO..E13	9.929	< 2e-16
E3,10	J.NO2.*Pressure	-3.613	0.000305
E4,5	ca.O3..E8*Solar.Elevation.Angle.5.hrs.ago	2	0.045533
E4,6	ca.O3..E8*Solar.Elevation.Angle	10.974	< 2e-16
E4,7	ca.O3..E8*Emis.g.s.	26.679	< 2e-16
E4,8	ca.O3..E8*JO1D.JNO2	-3.216	0.001307
E4,9	ca.O3..E8*ca.CO..E13	-19.787	< 2e-16
E4,10	ca.O3..E8*Pressure	10.307	< 2e-16
E4,11	ca.O3..E8*BLH	-6.656	3.00E-11
E5,6	Solar.Elevation.Angle.5.hrs.ago*Solar.Elevation.Angle	8.061	8.76E-16
E5,9	Solar.Elevation.Angle.5.hrs.ago*ca.CO..E13	-8.864	< 2e-16
E5,11	Solar.Elevation.Angle.5.hrs.ago*BLH	3.196	0.001398
E6,7	Solar.Elevation.Angle*Emis.g.s.	9.12	< 2e-16
E6,8	Solar.Elevation.Angle*JO1D.JNO2	14.426	< 2e-16
E6,9	Solar.Elevation.Angle*ca.CO..E13	-10.918	< 2e-16
E6,10	Solar.Elevation.Angle*Pressure	2.057	0.039734
E7,9	Emis.g.s.*ca.CO..E13	-19.435	< 2e-16
E7,10	Emis.g.s.*Pressure	-2.477	0.013284
E7,11	Emis.g.s.*BLH	3.592	0.000331
E8,9	JO1D.JNO2*ca.CO..E13	-6.404	1.61E-10
E8,10	JO1D.JNO2*Pressure	2.701	0.006925
E9,10	ca.CO..E13*BLH	5.747	9.46E-09
E9,10	ca.CO..E13*Pressure	-4.998	5.92E-07
E10,11	Pressure*BLH	6.415	1.49E-10

Table 17: Statistical output for the regression coefficients of integrated OPE for morning.

		t value	Pr(> t)
F0	(Intercept)	-0.352	0.725079
F3	J.NO2.	5.56	2.89E-08
F4	ca.O3..E8	-6.581	5.36E-11
F6	Solar.Elevation.Angle	5.614	2.12E-08
F7	Emis.g.s.	-5.998	2.19E-09
F8	JO1D.JNO2	-5.194	2.17E-07
F9	ca.CO..E13	4.143	3.50E-05
F11	BLH	2.553	0.010717
F1,3	Windspeed*J.NO2.	-2.239	0.025226
F1,5	Windspeed*Solar.Elevation.Angle.5.hrs.ago	2	0.045589
F1,8	Windspeed*JO1D.JNO2	6.769	1.51E-11
F3,4	J.NO2.*ca.O3..E8	-12.763	< 2e-16
F3,5	J.NO2.*Solar.Elevation.Angle.5.hrs.ago	7.665	2.27E-14
F3,6	J.NO2.*Solar.Elevation.Angle	-3.055	0.002266
F3,9	J.NO2.*ca.CO..E13	17.449	< 2e-16
F3,11	J.NO2.*BLH	3.785	0.000156
F4,5	ca.O3..E8*Solar.Elevation.Angle.5.hrs.ago	-5.453	5.27E-08
F4,6	ca.O3..E8*Solar.Elevation.Angle	3.21	0.00134
F4,7	ca.O3..E8*Emis.g.s.	14.034	< 2e-16
F4,8	ca.O3..E8*JO1D.JNO2	2.536	0.011252
F4,9	ca.O3..E8*ca.CO..E13	-18.022	< 2e-16
F4,10	ca.O3..E8*Pressure	6.534	7.28E-11
F5,7	Solar.Elevation.Angle.5.hrs.ago*Emis.g.s.	-4.09	4.40E-05
F5,8	Solar.Elevation.Angle.5.hrs.ago*JO1D.JNO2	-3.294	0.000997
F5,10	Solar.Elevation.Angle.5.hrs.ago*ca.CO..E13	5.789	7.66E-09
F6,10	Solar.Elevation.Angle*Pressure	-5.75	9.64E-09
F7,10	Emis.g.s.*ca.CO..E13	-10.748	< 2e-16
F8,9	JO1D.JNO2*ca.CO..E13	-14.334	< 2e-16
F8,10	JO1D.JNO2*Pressure	5.268	1.46E-07
F8,11	JO1D.JNO2*BLH	-3.174	0.001518
F9,10	ca.CO..E13*Pressure	-3.116	0.001845
F9,11	ca.CO..E13*BLH	-4.797	1.67E-06
F10,11	Pressure*BLH	-2.413	0.015877

C.2.2 Morning

The statistical output for the regression coefficients of the integrated OPE for morning are given in Table 17.

The residual standard error was 2.752 on 3620 degrees of freedom.

Multiple R-Squared: 0.71, Adjusted R-squared: 0.71.

F-statistic: 217.7 on 41 and 3620 DF, p-value: < 2.2e-16.

Residuals; Min: -18.312 , 1Q: -0.822, Median: -0.044, 3Q: 0.760, Max: 89.252

C.2.3 Evening

The statistical output for the regression coefficients of the integrated OPE for evening are given in Table 18.

The residual standard error was 1.309 on 4255 degrees of freedom.

Multiple R-Squared: 0.85, Adjusted R-squared: 0.84.

F-statistic: 494.6 on 47 and 4255 DF, p-value: < 2.2e-16.

Residuals; Min: -5.147, 1Q: -0.775, Median: -0.053, 3Q: 0.584, Max: 9.917

Table 18: Statistical output for the regression coefficients of integrated OPE for evening.

		t value	Pr(> t)
G0	(Intercept)	2.931	0.0034
G5	Solar.Elevation.Angle.5.hrs.ago	4.027	5.76E-05
G8	JO1D.JNO2	3.179	0.001488
G9	ca.CO..E13	-3.741	0.000185
G10	Pressure	-3.244	0.001186
G11	BLH	-4.505	6.83E-06
G1,2	Windspeed*Temp	6.968	3.72E-12
G1,4	Windspeed*ca.O3..E8	-4.879	1.11E-06
G1,5	Windspeed*Solar.Elevation.Angle.5.hrs.ago	6.709	2.22E-11
G1,6	Windspeed*Solar.Elevation.Angle	6.78	1.37E-11
G1,7	Windspeed*Emis.g.s.	-7.666	2.18E-14
G1,9	Windspeed*ca.CO..E13	4.416	1.03E-05
G1,10	Windspeed*Pressure	-2.727	0.006416
G1,11	Windspeed*BLH	4.924	8.79E-07
G2,4	Temp*ca.O3..E8	-4.054	5.13E-05
G2,6	Temp*Solar.Elevation.Angle	-2.735	0.006269
G2,7	Temp*Emis.g.s.	2.697	0.007025
G2,8	Temp*JO1D.JNO2	-2.4	0.016434
G2,9	Temp*ca.CO..E13	4.14	3.55E-05
G3,4	J.NO2.*ca.O3..E8	4.751	2.09E-06
G3,9	J.NO2.*ca.CO..E13	-3.356	0.000798
G4,5	ca.O3..E8*Solar.Elevation.Angle.5.hrs.ago	-15.055	< 2e-16
G4,7	ca.O3..E8*Emis.g.s.	11.44	< 2e-16
G4,8	ca.O3..E8*JO1D.JNO2	-4.778	1.83E-06
G4,9	ca.O3..E8*ca.CO..E13	-8.716	< 2e-16
G4,10	ca.O3..E8*Pressure	3.708	0.000212
G4,11	ca.O3..E8*BLH	-2.813	0.004938
G5,6	Solar.Elevation.Angle.5.hrs.ago*Solar.Elevation.Angle	20.907	< 2e-16
G5,7	Solar.Elevation.Angle.5.hrs.ago*Emis.g.s.	-9.055	< 2e-16
G5,8	Solar.Elevation.Angle.5.hrs.ago*JO1D.JNO2	-5.999	2.15E-09
G5,10	Solar.Elevation.Angle.5.hrs.ago*Pressure	-2.471	0.013528
G5,11	Solar.Elevation.Angle.5.hrs.ago*BLH	4.124	3.80E-05
G6,9	Solar.Elevation.Angle*ca.CO..E13	7.959	2.21E-15
G6,11	Solar.Elevation.Angle*BLH	2.402	0.01635
G7,9	Emis.g.s.*ca.CO..E13	-3.929	8.67E-05
G7,10	Emis.g.s.*Pressure	-3.087	0.002036
G9,10	ca.CO..E13*Pressure	2.211	0.027094
G10,11	Pressure*BLH	4.599	4.36E-06

References

- [Boersma et al., 2007] Boersma, K., Eskes, H., Veeffkind, J., Brinkma, E., van der A, R., Sneep, M., van den Oord, G., Levelt, P., Stammes, P., Gleason, J., and Buscela, E. (2007). Near-real time retrieval of tropospheric NO₂ from OMI. *Atmospheric Chemistry and Physics*, 7:2103–2118.
- [Charlton-Perez et al., 2009] Charlton-Perez, C., Evans, M., Marsham, J., and Esler, J. (2009). The impact of resolution on ship plume simulations with NO_x chemistry. *Atmospheric Chemistry and Physics*, 9:8587–8618.
- [Chen et al., 2005] Chen, G., Huey, L., Trainer, M., Nicks, D., Corbett, J., Ryerson, T., Parrish, D., Nueman, J., Nowak, J., Tanner, D., Holloway, J., Brock, C., Crawford, J., Olson, J., Sullivan, A., Weber, R., Schaufli, S., Donnelly, S., Atlas, E., Roberts, J., Flocke, F., Hübler, G., and Fehsenfeld, F. (2005). An investigation of the chemistry of ship emissions plumes during ITCT 2002. *Journal of Geophysical Research*, 110(D10S90).
- [Corbett et al., 1999] Corbett, J., Fischbeck, P., and Pandis, S. (1999). Global nitrogen and sulfur inventories for oceangoing ships. *Journal of Geophysical Research*, 104(D3):3457–3470.
- [Corbett and Kochler, 2003] Corbett, J. and Kochler, H. (2003). Updated emissions from ocean shipping. *Journal of Geophysical Research*, 108(D20):4650.
- [Corbett et al., 2007] Corbett, J., Winebrake, J., Green, E., Kasibhatla, P., Eyring, V., and Lauer, A. (2007). Mortality from ship emissions: A global assessment. *Environmental Science & Technology*, 41(24):8512–8518.
- [Davis et al., 2001] Davis, D., Grodzinsky, G., Kasibhatla, P., Crawford, J., Chen, G., Liu, S., Bandy, A., Thornton, D., Guan, H., and Sandholm, S. (2001). Impact of ship emissions on marine boundary layer NO_x and SO₂ distributions over the pacific basin. *Geophysical Research Letters*, 28(2):235–238.
- [DeMore et al., 1997] DeMore, W., Sander, S., Golden, D., Hampson, R., Kurylo, M., Howard, C., Ravishankara, A., and Kolb, C. (1997). Chemical kinetics and photochemical data for use in stratospheric modeling. *JPL-Publ.*, 97-4(Evaluation number 12).
- [EPA, 2000] EPA (2000). Analysis of commercial marine vessels emissions and fuel consumption data. Technical Report EPA 420-R-00-002, EPA, Washington D.C.
- [Evans and Jacob, 2005] Evans, M. and Jacob, D. (2005). Impact of new laboratory studies of N₂O₅ hydrolysis on global model budgets of tropospheric nitrogen oxides, ozone and OH. *Geophysical Research Letters*, 32(L09813).
- [Eyring et al., 2005] Eyring, V., Köhler, H., van Aardenne, J., and Lauer, A. (2005). Emissions from international shipping: 1. The last 50 years. *Journal of Geophysical Research*, 110.
- [Franke et al., 2008] Franke, K., Eyring, V., Sander, R., Hendricks, J., Lauer, A., and Sausen, R. (2008). Toward effective emissions of ships in global models. *Meteorologische Zeitschrift*, 17(2):117–129.
- [Freiberg, 1976] Freiberg, J. (1976). The iron catalyzed oxidation of SO₂ to acid sulphate mist in dispersion plumes. *Atmospheric Environment*, 10:121–130.
- [Hanna et al., 1985] Hanna, S., Schulman, L., Paine, R., and Pleim, J. (1985). Development and evaluation of the offshore and coastal dispersion model. *Journal of the Air Pollution Control Association*, 35(10):1039–1047.
- [Hobbs et al., 2000] Hobbs, P., Garrett, T., Ferek, R., Strader, S., Hegg, D., Frick, G., Hoppel, W., Gasparovic, R., Russel, L., Johnson, D., O’Dowd, C., Durkee, P., Nielsen, K., and Innis, G. (2000). Emissions from ships with respect to their effects on clouds. *Journal of the Atmospheric Sciences*, 57:2570–2590.
- [Hornik, 2009] Hornik, K. (2009). The R FAQ. ISBN 3-900051-08-9.
- [Kasibhatla et al., 2000] Kasibhatla, P., II, H. L., Moxim, W., Pandis, S., Corbett, J., Peterson, M., Honrath, R., Frost, G., Knapp, K., Parrish, D., and Ryerson, T. (2000). Do emissions from ships have a significant impact on concentrations of nitrogen oxides in the marine boundary layer? *Geophysical Research Letters*, 27(15):2229–2232.
- [Meijer et al., 1997] Meijer, E., van Velthoven, P., Wauben, W., Beck, J., and Velders, G. (1997). The effects of the conversion of nitrogen oxides in aircraft exhaust plumes in global models. *Geophysical Research Letters*, 24(23):3013–3016.

- [Melo et al., 1978] Melo, O., Lulis, M., and Stevens, R. (1978). Mathematical modelling of dispersion and chemical reactions in a plume - oxidation of NO to NO₂ in the plume of a power plant. *Atmospheric Environment*, 12:1231–1234.
- [Song et al., 2003] Song, C., Chen, G., Hanna, S., Crawford, J., and Davis, D. (2003). Dispersion and chemical evolution of ship plumes in the marine boundary layer: Investigation of O₃/NO_y/HO_x chemistry. *Journal of Geophysical Research*, 108(D4):4143.
- [Vinken, 2008] Vinken, G. (2008). Detecting and comparing NO₂ ship tracks from space using OMI and SCIAMACHY. BSc. Thesis, R-1736-S. Eindhoven University of Technology.
- [von Glasow et al., 2003] von Glasow, R., Lawrence, M., Sander, R., and Crutzen, P. (2003). Modeling the chemical effects of ship exhaust in the cloud-free marine boundary layer. *Atmospheric Chemistry and Physics*, 3:233–250.
- [Wang et al., 2008] Wang, C., Corbett, J., and Firestone, J. (2008). Improving spatial representation of global ship emissions inventories. *Environmental Science & Technology*, 42(1):193–199.